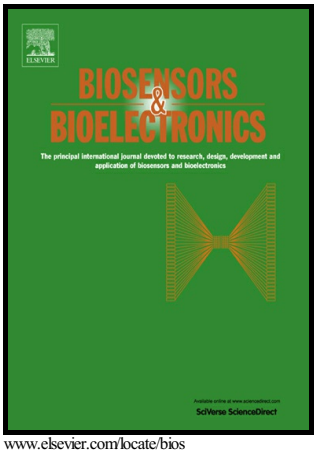

www.elsevier.com/locate/bios

PROGRESS AND CHALLENGES IN ELECTROCHEMILUMINESCENT APTASENSORS

Kateryna Muzyka, Muhammad Saqib, Zhongyuan Liu, Wei Zhang, Guobao Xu

PII: S0956-5663(17)30015-5
DOI: http://dx.doi.org/10.1016/j.bios.2017.01.015
Reference: BIOS9480

To appear in: *Biosensors and Bioelectronic*

Received date: 16 October 2016
Revised date: 16 December 2016
Accepted date: 6 January 2017

Cite this article as: Kateryna Muzyka, Muhammad Saqib, Zhongyuan Liu, We Zhang and Guobao Xu, PROGRESS AND CHALLENGES IN ELECTROCHEMILUMINESCENT APTASENSORS, *Biosensors an Bioelectronic,* http://dx.doi.org/10.1016/j.bios.2017.01.015

PROGRESS AND CHALLENGES IN ELECTROCHEMILUMINESCENT APTASENSORS

Kateryna Muzyka[a,b], Muhammad Saqib[a,c], Zhongyuan Liu[a], Wei Zhang[a*], Guobao Xu[a*]

[a]State Key Laboratory of Electroanalytical Chemistry, Changchun Institute of Applied Chemistry, Chinese Academy of Sciences, Changchun, Jilin 130022, People's Republic of China.

[b]Laboratory of Analytical Optochemotronics, Department of Biomedical Engineering, Kharkiv National University of Radio Electronics, Kharkiv 61166, Ukraine.

[c]University of Chinese Academy of Sciences, No. 19A Yuquanlu, Beijing 100049, China

Abstract

The importance of developing new diagnostic and detection technologies for the growing number of sensing challenges is rising each year. Here, we present a comprehensive and concise review on electrochemiluminescent (ECL) aptasensors by putting special emphasis on its characteristic features, advances, challenges, and applications of ECL based aptasensors. ECL is an ideal tool for constructing such sensors because of its inherent characteristics and can be easily integrated into aptamer based sensing platforms. This review summarizes the "synergistic benefits" of ECL aptamer-based sensors; classifications of ECL aptamer-based assay designs, and signal amplification strategies. This critical review highlights the effects of integration of nanomaterials, immobilization techniques, and amplification/detection strategies on the analytical performance of ECL based aptasensors. Moreover, several

proof-of-concepts with appropriate figures and explanations have been shown to provide a general guide for the design of ECL aptasensors, and to stimulate further application of these ECL aptasensors. Finally, we conclude with the remaining challenges and opportunities to inspire further developments in ECL aptasensors.

Abbreviations

(2,2′-bipyridine-4,4′-dicarboxylic acid)-ethylenediamine (**Ru1**); 1-hexanethiol (**HT**); 2-(dibutylamino)ethanol (**DBAE**); 3-Mercaptopropyltrimethoxysilane (**MPTMS**); 4-(dimethylamino)butyric acid (**DMBA**); 6-Mercapto-1-hexanol (**MCH**); Adenosine triphosphate (**ATP**); Aligned carbon nanotubes (**ACNTs**); Amino-terminated perylene derivative (**PTC-NH_2**); Assembling N-(aminobutyl)-N-ethylisoluminol functionalized gold nanoparticles (**ABEI-AuNPs**); ATP-binding aptamer (**ABA**); bis(2,2′-bipyridine)-4′-methyl-4′-methyl-4-carboxybipyridine ruthenium(II) complex (**Ru1***);

bis(2,2′-bipyridine)-4′-methyl-4-carboxybipyridineruthenium-*N*-succinimidyl-ester bis(hexafluorophosphate) (**Ru3**) $Ru(bpy)_3]^{2+}$ - N-hydroxysuccinimide ester (**Ru4**); Bovine serum albumin (**BSA**); Chitosan (**CTS**); Chloramphenicol (**CAP**); Chlorogenic acid (**CA**); Complementary ssDNA (**css-DNA**); Cyanine dye (**Cy5**); Cyclodextrins (**CD**); Diblock oligonucleotide (**d(Am-Tn));** Dibutyl ethanolamine (**DBAE**); Double strand DNA (**ds-DNA**); Electrochemiluminescence (**ECL**); Electrontransfer (**ET**); Employing loop-mediated isothermal amplification (**LAMP**); Ferrocene (**Fc**); Glassy carbon electrode (**GCE**); Glucose oxidase nanoparticles (**GOxNPs**); Gold nanoparticles (**AuNPs**); Grapheme oxide (**GO**); Graphene (**Gr**); Graphene sheets (**GS**); Hollow Au nanoparticles (**HAuNPs**); Horseradish peroxidase (**HRP**); Hyperbranched rolling circle amplification (**HRCA**); Low limit of detection

(**LoD**); Luminol-gold nanoparticles (**L-Au NPs**); Magnetic beads (**MBs**); Magnetic controlled gold electrode (**MCGE**); Malachite green (**MG**); Molecular beacon (**MBs**); Molecular beacon based aptamer (MBA); Molybdenum disulfide (**MoS_2**); Multiwalled carbon nanotubes (**MWNTs**); N-(3-dimethylaminopro-pyl)-N′-ethylcarbodiimidehydrochloride (**EDC**); N-(aminobutyl)-N-(ethylisoluminol) (**ABEI**); N-(aminobutyl)-N-(ethylisoluminol)/hemin dual-functionalized graphene hybrids (**A-H-GNs**); Nafion (**Nf**); Nanoparticles (**NPs**); N-hydroxysuccinimide (**NHS**); Nitrogen-doped grapheme quantum dots (**NGQDs**); Phenyleneethynylene derivative modified nanotubular mesoporous Pt–Ag alloy nanoparticles (**P-acid–Pt–Ag ANPs**) Platinum nanostructured networks (**PNNs**); poly(ethylenimine) (**PEI**); poly(pyrrole-*co*-pyrrolepropylic acid) nanoparticles (**Ppy-pa NPs**); poly-glycidyl methacrylate (**PHM**); Polymerase chain reaction (**PCR**); Polystyrene sulfonate (**PSS**); Pt nanoparticles (**PtNPs**); Quantum dots (**QD**); Reduced graphene oxide (**RGO**); Resonance energy transfer (**RET**); Rolling circle amplification (**RCA**); $Ru(bpy)_2^{3+}$ (**Ru**); $Ru(phen)_2(cpaphen)]2'$ linked N-(3-aminopropyl)methacrylamide (**Ru2**); Screen-printed carbon electrode (**SPCE**); Silica nanoparticles (**SNPs**); Single-stranded DNA (**ssDNA**); Single-walled carbon nanotubes (**SWCNTs**); Streptavidin (**SA**); Streptavidin–alkaline phosphatase (**SA–ALP**); Surface electron transfer resistance (**Rct**); Surface plasmon resonance (**SPR**); Template-enhanced hybridization processes (**TeHyP**); Tetrahedron-structured DNA (**ts-DNA**); Thioglycolic acid (**TGA**); Thrombin aptamer (**TBA**); Thrombin aptamer I (**TBA I**); Thrombin aptamer II (**TBA II**); Tripropylamine (**TPA**); Tris(2,2′-bipyridyl) ruthenium(II) (**Ru**); Tris(2,2′-bipyridyl)ruthenium(II)-doped silica nanoparticles (**RuSiNPs**); Tris(4,4′-dicarboxylicacid-2,2′-bipyridyl) ruthenium(II)dichloride (**Ru5**)

***Keywords**:* aptasensor, electrochemiluminesence, structure-switching, hybridization, complementary DNA, intercalation, quenching, adsorption, amplification, energy transfer

1. Introduction

The detection of important molecules, including proteins (biomarkers), toxins, drugs, antibiotics, pollutants, heavy metals etc. has increased demand to design and develop high-performance analytical tools. However, the majority of such molecules do not possess the necessary properties (e.g. electroactivity, fluorescence) themselves, and thus cannot be determined directly by means of existing physical and chemical methods. This problem can be overcome by employing ***biosensors*** that can detect substances via the detection of binding events between target molecules and recognition elements with a further transduction of these events into an analytical physicochemical signal (Vigneshvar, 2016). It is worthwhile to mention that ***recognition element*** defines the basic characteristic of biosensors – *specificity* (selectivity). In turn, the role of a ***transducer*** is to ensure high *sensitivity*.

Until now, ***monoclonal antibodies*** have been regarded as the gold-standard recognition elements in biosensors (Sharma, 2016), which is attributed to their high binding affinity and extraordinary specificity. Production of antibodies is conceptually simple. However, results are not entirely predictable because it depends upon such a complex biological system (immunity of a living organism) (Germain, 1986). Moreover, antibodies are unstable in

non-physiological conditions. To the best of our knowledge, the production of antibodies against some haptens (low-molecular-weight compounds), such as poison, are still absent or at least limited. It is because such high-toxic molecules of non-protein nature can block immune response even to the hapten-carrier adduct.

Aptamers (the Latin word aptus (meaning "to fit")), as synthetic, typically <100 mer *single-stranded DNA* (ss-DNA) or RNA ligands (Ellington and Szostak. 1990; Tuerk and Gold, 1990), are free from above mentioned limitations, and possessed antibody-like specificity. Moreover, in comparison to antibodies, aptamers possess the following key *advantages*: i) they are of 5–25 KDa molecular weight; and 1–2 nm in size vs. 150 kDa and 10 nm for antibodies; ii) their small sizes enable aptamers to bind onto hidden epitopes, which cannot be targeted by antibodies; iii) it is easier to synthesize and modify aptamers in vitro. Due to their outstanding properties, aptamer emerges as a new generation of recognition element for sensing applications (Chen and Yang, 2015a; Sun and Zu, 2015; Chen et al., 2016b; Witt et al., 2015).

In order to obtain high sensitivity, efficient transduction techniques should be sought to monitor successful binding events between target analytes and aptamers. Owing to the several appealing features, ***electrochemiluminescence*** (ECL) offers an attractive transduction strategy in antibody-based biosensors (Muzyka, 2014). For example, it possesses *low limit of detection* (LoD) (even without amplification); it has *high potential for miniaturization*, *in-situ* analysis and *multichannel detection*. Overviews focused on general mechanism and recent advances in ECL were available in a fundamental book (Bard, 2004) and some recent reviews (Liu et al. 2015). Interestingly, since the inception of ECL

aptasensor about 10 years ago (Wang et al., 2007), a growing number of ECL 'aptasensors' proof-of-concepts have been developed; but only partly reviewed in some reviews (Liu et al. 2015; Yuan et al., 2011; Yin, 2012; Ravalli et al. 2016). In order to improve the performance and stimulate the evolution of ECL aptasensors, it is helpful to have a more systematized knowledge about their *status quo*.

Thus, the present review will summarize existing ECL-aptasensors platforms in a systematic manner, describe and critically analyse their conceptual framework, define new trends, as well as provide database-like information on performance of ECL aptasensors.

2. Basic strategies of ECL aptamer-based assay

2.1 Classification, based on target binding site number: single-site and dual binding site (sandwich) assay formats

Like antibodies, folded aptamers have the ability to recognize unique *epitope* (*binding sites*) of target analytes via specific sequence of hydrogen bonding between the bases and amino acid side chains, spatial adjustment, electrostatic interactions, van der Waals forces and interaction between aromatic groups (π–π stacking) (Jarczewska, 2016). A classification of ECL aptamer-based assays is essential on the bases of *number of binding sites*, which possess a target molecule.

Large molecules (usually with a molecular weight larger than 1000 D) are structurally complex and provide the distinct epitops and each of them is complementary to individual paratope of aptamer. This allows both *single*- and *dual-site* ("sandwich") *binding* assay formats.

Usually, the sandwich-type assay (see Fig. 1) employs a pair of aptamers (capture and reporter). In general, one end of ***capture aptamer*** (probe) is anchored onto the electrode surface (in majority cases, Au electrode, because it allows the thiol chemistry for immobilization), and the other end provides affinity interaction with a complementary binding site of target molecule. In turn, one end of the ***reporter probe*** is usually conjugated with an ECL-label (e.g., ruthenium complexes, and its derivatives, such as *N*-hydroxysuccinimide (NHS) ester, phosphoramidite conjugates, quantum dots (QD), and nanoparticles (NPs). The other end of reporter probe provides affinity recognition.

A sandwich assay exhibits higher specificity than an assay with a single affinity site. This is because target must be recognized independently by two different aptamers, rather than by one, before transduction of binding event into ECL analytical signal. Data on the performance of aptamer-based ECL assays in sandwich design is presented in Table 1.

In general, sandwich-type ECL aptamer assays are performed for the *large molecules*, and it is still challenging to develop aptamer-based (as well as antibody-based) sandwich assay system for the detection of ***small molecules*** (upper molecular-weight limit ~900 D (Ruscito and DeRosa, 2016)) which usually possessed only one epitop. To address this issue, Stojanovic et al. (2000) developed a ***split-aptamer-based strategy*** in which nucleic acid aptamers were split into two fragments to specifically form a ternary complex in the presence of target. Two separate oligonucleotides do not have secondary structure, thereby preventing false positive or non-specific signals.

To obtain positive signals, the two split aptamer fragments must be drawn close to each other, which is possible only when the probes bind to a target. This elegant

so-called ***"sandwich-like" approach*** was adapted in ECL aptasensors for the detection of small targets, such as *adenosine triphosphate* (ATP) and cocaine (see Table 2). As shown in Table 2, the LoD of small molecules for sandwich-like detection is in pM range, and is comparable with several reports of single-site detection for such molecules (see Tables 3). For example, Yan et al. (2013) have adapted "sandwich-like" approach in *microfluidic origami ECL aptasensor* for ATP detection, and reached LoD as low as 0.1 pM. One fragment with a thiolated 5′-end of a split single aptamer was immobilized onto the surface of the AuNPs layer via thiol–Au interaction. Another fragment with the amine 3′-end was labeled with ECL-tag. ATP-target triggered the partial hybridization of the two fragments, which led to increasing concentration of ECL-tag in the paper sample zone and resulted in ECL emission.

As pointed out in earlier review (Chen et al., 2016a), split aptamers have significant potential in the development of sandwich aptasensors. However, effective methods for splitting aptamers into suitable fragments are still scarce. To date, more than 100 types of small-molecule-binding aptamers have been reported, but only about six of them have been successfully constructed into split aptamers. For the detection of small molecules ***single-site assay formats*** are more preferable, and can be broadly classified into label-based and label-free. *Label-based detection* relies on the specific properties of labels for detecting a particular target. In contrast, *label-free detection* is suitable for the target molecules that are not labeled or for the screening of analytes which are not easy to tag.

2.2 Labeled-based ECL aptasensors platforms

2.2.1 Aptamer-labeled ECL platforms based on quenching effect

It has been reported that *ferrocene* (Fc) can effectively quench the ECL emission of $Ru(bpy)_3^{2+}$ at the electrode surface via energy or electron transfer between $Ru(bpy)_3^{2+*}$ and Fc^+ (the oxidation state of Fc). Notably, the quenching of the ECL emission occurs only when the Fc^+ and $Ru(bpy)_3^{2+*}$ moieties are in close proximity (Cao et al. 2006). By utilizing the combination of above mentioned principle and the specific features of the aptamers, different ECL aptasensors platforms can be developed.

a) Sensing platforms based on ECL quenching effect via target induced structure-switching of Fc-labeled aptamer

Molecular beacon **based** ***aptamer*** (MBA) is a useful approach to change the separation distance between ECL luminophore and quencher. As a hairpin shaped molecule, *molecular beacon* (MB) can undergo spontaneous conformational change following hybridization with the complementary nucleic acid and was initially described in 1996 (Tyagi and Kramer, 1996). As shown in Fig. 2, a typical MB structure can be divided into 4 parts: 1) loop, an 18–30 base pair region that is complementary to the target sequence; aptamers are employed in the engineering of the loop region; 2) stem; 3) an ECL reporter and 4) a quencher covalently attached to the 5′ or 3′ end of the aptamer stem respectively.

Wang et al. (2009) have adapted labeled MBA in the development of solid-state ECL sensing platform which was applied for thrombin detection (LoD = 50 fM; working range: 0.1 pM to 100 pM). In the proposed system, a complex of gold NPs (AuNPs) and ($Ru(bpy)_3^{2+}$) immobilized onto Au electrode have been used *to emit ECL*, and Fc-MBA *to control the ECL emission*. Upon the reactions with the target, the MBA opened its stem-loop, and the labeled Fc was consequently kept away from

the ECL substrate. Such structural change resulted in an obvious ECL intensity increment due to the decreased quenching effect of Fc to the ECL substrate (Fig. 3).

A drawback of these systems is the relatively short-scale conformational freedom of immobilized MBA. Thus, due to the limited distance between the ECL substrate and quencher, the working range of concentration for aforementioned type of the sensing platform was narrow (e.g. 3 and 1 orders of magnitude for thrombin and adenosine (Wang et al. (2009; 2010), respectively). In order to solve the above-mentioned problem, Liao et al. (2011a) reported a strategy, where Fc-labeled MBA could be regarded as infinitely distant from the ECL substrate, as MBA was in the solution before interaction with the target. Because of increase in conformation freedom of MBA, it was possible to achieve working range of thrombin detection up to 4 orders of magnitude (5 pM to 50 nM).

Even though the introduction of MB in aptasensors has provided unique possibility of utilizing the conformational change strategies, there are still some significant drawbacks with MBA-based ECL sensors (Zheng et al., 2015), such as the probability of false opening of the MBA probe, requirement of extra chemical modification (with the Fc and ECL labels) that can affect the affinity of MBA, requirement of prior knowledge of secondary or tertiary structure of aptamer for providing high affinity interaction with a target molecule, quite slow sensor response (due to relatively slow (~1 hour) target-induced conformation change).

b) Sensing platforms based on ECL quenching effect via target induced displacement of Fc-labeled aptamer

One of the important property of aptamers (as ss-DNA) is the possibility to *hybridize with* ***complementary ss-DNA*** to form a rigid ***double-stranded DNA*** (ds-DNA). Moreover, ds-DNA can be utilized for any aptamer without prior

knowledge of its secondary or tertiary structure. Since the interaction between aptamer and target is stronger than that between aptamer and its complementary DNA chain, aptamer –target interaction would lead to dissociation of ds-DNA.

Chen et al. (2010) have utilized this principle in a "*signal on"* ECL strategy (Fig. 4) which was applied for adenosine detection. *css-DNA* labeled with ECL tag (Ru-doped silica nanoparticles (Ru-SNPs)) was immobilized onto the Au electrode via Au–S interaction. In turn, Fc-labeled aptamer attached to the Au electrode through hybridization with the css-DNA to form ds-DNA. Hence the *quencher* (Fc) became closer to the *ECL reagent* (Ru-SiNPs), which led to the appearance of a weak ECL signal. In the presence of adenosine, the Fc-labeled aptamer released from the electrode surface, accompanied by the recovery of a strong ECL signal.

Fig. 5 depicted a similar approach. Instead of labeling of css-DNA, ECL luminophore was immobilized onto electrode to form solid-state ECL substrate. Moreover, beside the dissociation of the ds-DNA, the structure switching of the MB-contained aptamer took place after the addition of target (adenosine).

Compared with aforementioned ECL aptasensors, the proposed sensor had higher LoD (5 nM vs. 31 pM for (Chen et al., 2010)). Such difference was attributed to high background signals of solid-state ECL substrate. Moreover, due to the problem of limited signal gain, the linear response range of the above mentioned "signal off" approach was narrower (10 nM to 0.1μM) vs. (50 nM to 0.1 nM) than "signal on" approach proposed by Chen et al. (2010).

Shi et al. (2014) have fabricated an adenosine aptasensor based on target-induced displacement of Fc-labeled aptamer with utilization of ***ITO bipolar electrode concept*** (Bouffier et al., 2016). As shown in Fig. 6, both oxidation and reduction reactions occur simultaneously on the same bipolar electrode. The Fc group was kept in close

contact with the electrode surface to facilitate the electron transfer between Fc and the electrode. Fc-labeled aptamer was utilized to promote the reduction reaction on the cathode, which accelerates the oxidation reactions of $Ru(bpy)_3^{2+}$ / tripropylamine (TPA) system on anode. Simultaneous increase in faraday current through bipolar electrode has resulted in ECL enhancement at anode (according to the electric neutrality of bipolar electrode). In the presence of target adenosine, ECL signal decreased by the target-induced removal of Fc-aptamer on the cathodic pole. The proposed system has showed remarkable (8-fold change in ECL emission) dynamic range, and sensitivity (1 fM) for adenosine detection due to low background signal.

It can be concluded that ECL platforms based on *the ECL quenching effect via target induced displacement* of Fc-labeled aptamer are more useful, because of the less restricted conformational requirements to aptamer. Therefore, this strategy can be easier adapted for the determination of wide range of targets than previous one. Moreover, this strategy is faster than MBA-based, as about 20 min are required for the target-induced cssDNA displacement (according to aforesaid examples). However, realization of such platform requires some specific steps, such as the hybridization reaction of aptamer and cssDNA. It is important to mention that every additional step needs more time, and inherently contains sources of variability, which in turn results in variability in the test results.

c) Sensing platforms based on change of ECL response via target induced alteration of interactions between labeled aptamer and carbon materials

Graphene and *graphene-based materials* could significantly improve and diversify the performance of ECL aptasensors. In particular, ***graphene oxide*** (GO) has several attractive properties from the point of view of ECL apta-assay. First, GO can strongly *adsorb ss-DNA* via *π-stacking interactions* between the ring structures in the

nucleobases and the hexagonal cells of GO. Second, GO has a high *ECL quenching ability*. Third, GO is *water soluble*. Taking advantages of this material, Huang et al. (2015) have developed a "signal on" strategy for ATP detection based on the adsorption and desorption of ECL-tag-labeled aptamer to the GOs (Fig. 7). Briefly, the formation of target-aptamer high affinity complex (instead of noncovalent aptamer-GO binding) has resulted in increased separation distance between GO and ECL-tag labeled aptamer, and decreased ECL quenching. The efficiency of above-mentioned approach has been proved during ATP detection (LoD = 4.8 pM; working range: 10 pM to 10 nM). The high sensitivity is attributed to the high quenching efficiency of GO.

Jin et al. (2013) reported a strategy where ECL-tag-labeled aptamers were adsorbed onto magneto-controlled magnetic GO nanosheets (dissolved in bulk solution) instead of immobilization onto electrode, and then they were attached to the electrode under the influence of magnet. After the binding with the target, aptamer was desorbed from GO nanosheets and diffused into the solution, eliminating influence of quenching effect. The system has been applied for the determination of thrombin (LoD=1.3 nM; linear response range: 2 nM to 50 nM). The reasons of the weak signal (and subsequently, narrow working range) for the proposed example can be summarized as following: *firstly*, a relatively long quenching distance of GO (up to 30 nm has been reported (Swathi and Sebastian, 2009)); *secondly*, probably slow diffusion of newly formed affinity target-aptamer complex, and thus, low separation distance from GO.

Li et al. (2014a) reported a "signal off" ECL aptasensor based on property of single-walled carbon nanotubes (SWCNTs) to show variable response in the presence of folded and unfolded aptamers. Initially the ECL-tag labeled aptamer was adsorbed onto SWCNT. The conformation of aptamer was changed after the formation of

target-aptamer complex, resulting in the displacement of ECL-tag-labeled aptamer from SWCNT-modified electrode and a decrease in ECL response (Fig. 8). The low LoD of adenosine (50 pM) can be attributed to the introduction of SWNTs into the ECL aptasensor that increased the number of ECL probes per binding event.

Thus, the *ECL sensing platforms based on adsorption and desorption* of ECL-tag-labeled aptamer to the carbon nanomaterials is a promising approach to design "one-shot" ECL aptasensors. However, it is necessary to keep in mind that false positive results can be arised, as many ions can mediate electrostatic interactions between a negatively charged surface and the aptamers nucleotides. Moreover, the steric requirements are necessary for the proper folding of aptamer, and consequently the affinity recognition of target is challenging due to strong interaction between aptamers' nucleobases and carbon materials. It should be noted that saturation adsorption of the ECL probe onto carbon materials would significantly affect ECL intensity, and thus affected sensitivity and working range.

d) Sensing platforms based on ECL quenching effects via "junction-probe" strategy

Zhang et al. (2011) utilized idea of *"junction-probe" strategy* to fabricate ECL aptasensor, and proved its sensitivity during thrombin detection (LoD=8.0 fM). The ECL aptasensor consisted of two main parts: an *ECL substrate* (AuNPs-Ru(bpy)$_3^{2+}$ composite onto Au electrode) and an *ECL intensity switch*. The ECL intensity switch contained three probes designed according to the "junction-probe" strategy, including *capture probe, aptamer probe,* and *Fc-labeled probe* (Fig. 9). In the presence of target (thrombin), the aptamer–target complex was formed and led to the reattachment of Fc-labeled probe from the "Y" junction structure. The residuary part of "Y" junction (capture and aptamer probes) was not stable due to its limited complementarity (usually 4–6 base pairs). Thus, the Fc was easily removed from the electrode surface

after washing with buffer solution and resulted in enhanced ECL intensity. The proposed strategy demonstrated much lower LoD (8.0 fM) than the existing ECL aptamer biosensors for thrombin detection (see Tables 1, 3). However, the working range of detection was not very wide (about 3 orders of magnitude). This can be explained by spatial restriction of the "Y" junction configuration, which limits the possibility to achieve the high parking density of DNA. On the other hand, higher density of "Y" junction DNAs hindered the reaction of TPA with $Ru(bpy)_3^{2+}$, and thus decreased the sensitivity. Zhang et al. (2009) reported that the surface density of 1.1×10^{12}–1.6×10^{12} molecules/cm^2 can provide stable hybridization efficiency and higher sensitivity for junction-probe biosensors. In term of sensors simplicity, formation of the "Y" junction configuration of DNA requires supplement steps and time that may be a reason of variability in the test results.

It can be concluded from subsection 2.2.1 that the aptamer-labeled ECL platforms based on the quenching effect can be successfully utilized for the detection of any target. Unfortunately, the real samples usually contain some potential ECL quenchers that can be serious obstacle in practical applications of quenching effect based platforms. However, due to the generation of ECL close to the electrode surface, the solution phase interferences can be avoided. Therefore, ECL technique is less affected from the potential quenchers in solution phase as compared to fluorescent and chemiluminescent techniques (Forster and Keyes, 2013). Thus, in this context ECL detection is more advantageous for aptasensors.

Another disadvantages related to the *label-based strategies* is alteration of the aptamer recognition ability after chemical-labeling. Other reports about signal tag labeled-on the complementary to aptamer ss-DNA, not on the aptamer are described in the next sub-section.

2.2.2 ss-DNA labeled ECL platforms based on change in separation distance between ECL-reporter and electrode (Quasi label-free approach)

As mentioned in the previous subsection, the ability of an aptamer to hybridize with the css-DNA to form ds-DNA, and to dissociate in the presence of a target can be used for its quantification purpose. This approach can also be utilized in so-called "*quasi label-free approach*", in which only labeling of css-DNA takes place. To the best of our knowledge, the first ECL aptasensor based on this idea was reported by Wang et al. (2007). Since the interaction between aptamer and target was stronger than that of aptamer and its css-DNA, the replacement of ECL-tag-labeled DNA probe by target was easy. This resulted in remarkable decrease in ECL signal (Fig. 10). Low LoD (1.0 fM) of thrombin have been achieved due to the large number of $Ru(bpy)_3^{2+}$molecules (onto SNPs) per binding event. Wang et al. (2015) also reported the similar strategy for the detection of small molecule (ochratoxin A), and achieved LoD as low as 1.24 pM.

"Signal on" detection platform based on target induced displacement of the labeled css-DNA (see Fig. 11) have been reported by Yao et al. (2009). This platform have been applied for the ECL based detection of ATP (LoD=0.02 nM; working range: 0.05 to 10 nM). This approach follows some similar steps as reported before (see Fig. 10). In both cases, modified (with ECL-labeled ds-DNAs) electrodes exhibited negligible ECL. However, both reports demonstrated different strategies in the presence of target molecules. In "signal off" strategy, the displacement of ECL-tag-labeled css-DNA resulted in increase in separation distance from the electrode surface, and ultimately decreased the ECL intensity. In contrast, in "signal on" strategy, ECL-tag-labeled css-DNA fixed onto the electrode surface. After incubation in a high ionic strength solution, stem loop structure was obtained. This

brought the ECL elements closer to the electrode surface, and resulted in enhancement in ECL intensity. In order to achieve high sensitivity and wide dynamic range, it is desirable to optimize conditions for strong initial ECL signal, e.g. via increasing surface density of receptors, or by decreasing a separation distance between ECL-label and electrode (e.g. via utilizing shot ss-DNA). In the second approach, it is advantageous to utilize weak initial ECL signal, e.g. through exploring a longer ss-DNA.

Li et al. (2014b) have reported a target induced strand displacement approach by introducing an *auxiliary probe* (see Fig.12) for the detection of thrombin (LoD = 2 pM; working range: 5 fM to 5.0 pM). The ECL aptasensor was fabricated by self-assembling a thiolated capture probe on the surface of gold electrode. Then the ECL probe was hybridized with the capture probe. Afterwards, the auxiliary probe was self-assembled on the surface of Au electrode. After bonding of thrombin with the capture probe, the part of the dehybridized ECL probe was hybridized with the neighboring auxiliary probe. As a result, the tagged ruthenium (II) complex came into close contact with the electrode surface. Thus, an increase in the ECL intensity was observed.

In order to improve the sensitivity of aptasensors based *on target-induced strand displacement strategy*, the css-DNA or aptamer duplex are commonly labeled with some other materials that can enhance the signal response. For instance, 4-(dimethylamino) butyric acid (DMBA) is a coreactant similar to TPA that displayed strong ECL signals with $Ru(bpy)_3^{2+}$. Gan et al. (2012b) used this feature of DMBA for ECL aptasensor to enhance the intensity of solid-state $Ru(bpy)_3^{2+}$ ECL biosensor for the detection of thrombin (LoD=0.4 pM). Huang et al. (2010) employed QDs–

labeled-css-DNA in ECL aptasensor for the first time for the detection of ATP (LoD=6 nM; working range: 0.018 to 90.72 mM).

Thus, it can be concluded that *the quasi label-free approach based on target induced strand displacement strategy* is easy to generalize for any aptamer. Also, it can expand the range of targets, including the live cells (Yu et al., 2011; Ding et al., 2012; Chen et al. 2014b). All critical aspects of this approach are similar to those have been discussed in subsection 2.2.1 b. However, in terms of selectivity and sensitivity, quasi-labeled approach is more beneficial, because non-labeled aptamer possessed better recognition ability.

2.3 Label-free ECL aptamer-based assay formats

2.3.1 Label-free detection based on the target induced blocking of the surface of ECL substrate

The main idea of this strategy can be summarized as: target-aptamer affinity complex produced by intermolecular recognition can *hinder the electron* transfer between ECL luminophore and co-reactant that results in decrease in the ECL intensity, and helps in the quantification of the target. Based on this mechanism, several ECL aptasensors have been developed.

In most published papers, ion-exchangeable polymer (Nafion) films are utilized for the immobilization of ECL substrate on the surface of glassy carbon electrode (GCE) of aptasensor. Nafion is resistant to strong oxidants at elevated temperature, but has a slow electron-transfer rate (Gui et al., 2014). Therefore, in order to improve ECL aptasensors performance, the researchers put strong efforts to overcome the drawbacks by doping NPs into the pure Nafion film. The composite film had more open structures, larger surface areas and provided conducting pathways for the

electron transfer. For example, Shi et al. (2014a) doped Nafion / L-cysteine film with AuNPs for the determination of carcinoembryonic antigen with a LoD of 3.8 pg mL^{-1}. Gui et al. (2014) have utilized $Ru(phen)_3^{2+}$@CNTs-Nafion composite film for the construction of a label-free ECL aptasensor for the sensitive detection of thrombin (LoD = 0.33 pM). Liu et al. (2014b; 2014c) have achieved LoD for thrombin up to 0.22 pM and 3.6 fM respectively. In the first report, HGNPs / Nafion-dopamine-melanin colloidal nanospheres – AuNPs were utilized as a composite film; while in the second report, Nafion – molybdenum sulfide (MoS_2) – graphene / MoS_2–graphene nanocomposites were utilized as a matrix for $Ru(bpy)_3^{2+}$. The low sensitivity in the later example can be attributed to the larger concentration of immobilized $Ru(bpy)_3^{2+}$, because of high loading capacity of MoS_2–graphene nanocomposite with flowerlike structure. However, the later report is advantageous due to cost-effective strategy for nanocomposite preparation.

Liao et al. (2011b) have doped Pt NPs with $Ru(bpy)_3^{2+}$–Nafion film to construct an aptasensor for the ultrasensitive determination of thrombin (LoD=0.33 fM). The Pt NPs doped $Ru(bpy)_3^{2+}$–Nafion film successfully inhibited the migration of $Ru(bpy)_3^{2+}$ into the electrochemically hydrophobic region of Nafion. It facilitated the electron transfer between $Ru(bpy)_3^{2+}$ and electrode surface. They utilized the biotin–streptavidin system for the enrichment of aptamers. It should be noted that the dissociation constant of the streptavidin-biotin complex is very low (10^{-15} M), and the complex is kinetically stable (Piran and Riordan, 1990). Therefore, this approach offers a fast, reliable and simple immobilization of biotinylated aptamers. Holmberg et al. (2005) have reported that the biotin-streptavidin interaction can be reversibly changed at elevated temperatures. Therefore, the streptavidin solid support can be re-used. However, similar to other proteins, streptavidin can undergo denaturation.

Therefore, aptasensors based on the streptavidin-coated slides could be degenerated over time even in chilled storage (Witt et al., 2015).

Yang et al. (2011) have developed a solid-state label-free aptasensors by utilizing CdS QDs / aligned carbon nanotubes electrode for the detection of thrombin with LoD up to 50 fM, which was one order of magnitude higher than the previously reported LoD by Liu et al. (2014a). The possible reason is that, the ECL intensity of CdS QDs is lower than that of the conventional luminescent reagents such as luminol or $Ru(bpy)_3^{2+}$.

Thus, it can be stated that the *ECL aptasensors based on blocking of the surface of ECL substrate* are useful platform. Because they did not required chemical labeling and can be re-used. However, such systems have relatively high background ECL signals, which can affect the sensitivity.

2.3.2 Label-free detection based on the intercalation of ECL luminophore to double-strand DNA structure

It is well known that the helical ds-DNA has the capacity to be *intercalated* with some small molecules into its grooves with high affinity. For example, Yin et al. (2009) have reported that $Ru(phen)_3^{2+}$ can be intercalated into the ds-DNA with a binding constant 1.24×10^4 M^{-1}. Afterwards, this property was utilized by them to design an ECL aptasensor for the detection of thrombin (LoD=0.02 pM). The general principle of *intercalation-based approach* includes following steps: adsorption of an aptamer on the electrode surface; formation of the ds-DNA between aptamer and its css-DNA; intercalation of $Ru(phen)_3^{2+}$ into the ds-DNA sequence; target-induced dissociation of ds-DNA; release of $Ru(phen)_3^{2+}$ into the solution; decrease in ECL emission (Fig.13).

Hu et al. (2009) have demonstrated that the introduction of DNA into the system can enhance the ECL intensity of $[Ru(bpy)_2dppz]^{2+}$ nearly ~1000 times. This property can be utilized to provide a sensitive protocol for the determination of analytes that can compete with $[Ru(bpy)_2dppz]^{2+}$ for intercalation into ds-DNA segments.

The possible limitation of the aptamer-based ECL sensors is restricted target accessibility due to surface-induced perturbation of the aptamer structure. Bu et al. (2013) have employed *tetrahedron-structured DNA* (ts-DNA) and a functional oligonucleotide during the development of the intercalation-based ECL aptasensor (Fig. 14). However, forenamed approach provided moderate sensitivity for ATP detection (LoD=0.2 nM) in comparison with other reports (see Table 3).

Zhao et al. (2011) have reported a *duplex-DNA-based* ECL aptasensor for cocaine detection (LoD=0.2 pM). The distinctive feature of this strategy is the formation of a partial double strand part with consequent intercalation of $Ru(phen)_3^{2+}$ *after* aptamer-target interaction (see Fig. 15). The background signal and false positives were lower than the previously reported aptasensors, because the ECL response is produced from the probe intercalated into the induced duplex during the recognition process.

The above mentioned *label-free intercalation-based examples* can be summarized as follows: no chemical labeling (which is quite time consumption procedure) is required so it can increase the sensitivity. The signal generation is independent of the special conformational changes so the number of targets can be extended. The concentration of luminophore for complete intercalation of the DNA grooves determined the sensitivity and working range. The higher concentration of ECL luminophore (e.g. $Ru(phen)_3^{2+}$) than concentration at complete intercalation can obviously increase the ECL background signal. The competition of ECL-probe with

other molecules "potential intercalaters" for the intercalation in ds-DNA has limitation for real samples analysis.

2.3.3 Other less widespread kinds of label-free target ECL detection

Recently, researches paid much attention to modify the sensors design by utilizing *stimuli-responsive materials*. For example, Chen et al. (2015b) have reported a label-free ECL aptasensor by utilizing a polyelectrolyte (Au–g-C_3N_4) film, which increased the permeability for the diffusion of coreactants after target-induced conformational change of aptamer. Advantage of this strategy was the low background signal due to the effective blockage of coreactant in the absence of target molecules. The LoD for bisphenol A was achieved as low as 0.05 $ng*mL^{-1}$ by using this strategy.

The host–guest recognition ability of cyclodextrins (CD) with respect to aptamer has been utilized in the design of new label-free ECL-based aptasensor (Chen et al., 2014c). In presence of target, the formation of aptamer–thrombin bioaffinity complexes restricted the recognition activities between aptamer and tris(bpyRu)-β-CD. Thus, less tris (bpyRu)-β-CD was immobilized onto the surface of GCE. It resulted in obvious decrease in ECL signal. The proposed ECL-based aptasensor exhibited excellent LoD for the detection of thrombin (0.1 pM) without labeling and amplification procedures.

Aptamers, as *nucleic-acid based molecules,* are *susceptible to the action of* a specific type of enzyme (***DNA ligase)***, which facilitates the joining of DNA strands together by catalyzing the formation of a phosphodiester bond. For example, the ATP-dependent ligase is inactive until it binds with a molecule of ATP, which leads to the loss of the pyrophosphate moiety from ATP and the formation of a covalent enzyme. The enzymatic ligation reaction shows specific

dependence on its cofactor ATP. Zhao et al. (2016) designed a new label-free ECL aptasensor for the detection of ATP based *on the aptamer–target interaction induced ATP-ligation.* In comparison with the reported methods for ATP detection, the proposed strategy showed an outstanding sensitivity for ATP (LoD=20 pM) because of the unique role of the ATP cofactor in the ligation reaction. However, this strategy cannot be applied for wide range of targets, because a potential target should be a cofactor of the enzymatic ligation reaction.

Several aptamers, DNA aptamers in particular, are known to contain a non-canonical nucleic acid structure (***G-quadruplex***). G-quadruplex structures are formed in nucleic acids by guanine rich sequences. Four guanine bases can associate to form a square planar structure called a guanine tetrad, and two or more guanine tetrads can stack on top of each other to form a G-quadruplex. One way of inducing or stabilizing G-quadruplex formation is to introduce a molecule which can bind to the G-quadruplex structure. For this purpose, a number of ligands such as small molecules and proteins have been developed. It has become an increasingly growing field of research (Simonsson, 2001), including ECL aptasensors. Thus, ECL aptasensors based on *target induced generation of the G-quadruplex structure* have been used for detection of ions (Pb^{2+}) up to pM level. For example, Wei et al. (2014) have utilized the G-quadruplex of aptamer probe for the "signal on" ECL sensor for Pb^{2+} (LoD=37.4 pM). The principle of this detection strategy is depicted in Fig. 16. In the presence of Pb^{2+}, the G-rich hairpin aptamer probe opened the stem-loop and formed the G-quadruplex. This phenomenon exposed the amino group that could covalently link to CdS QDs (ECL-labels) with the help of carboxyl groups on the surface, and resulted in increase in ECL intensity.

ECL aptasensors based on the G-quadruplex are promising for the determination of ions, but the aptasensors usually possess a quite narrow working range (near 2 orders of magnitude (see Table 3)). Interestingly, a wider working range for Pb^{2+} detection was achieved (5 order of magnitude) by combination of G-quadruplex approach with the ECL resonance energy transfer (Lei et al., 2015).

3. ECL aptamer sensing platform based on energy transfer

Nowadays, ECL energy transfer based detection platforms have received much attention in the determination of ion, protein, and DNA. For example, Wang et al. (2011) reported surface plasmon induced ECL enhancement of CdS nanocrystal thin films by AuNPs for the first time. They applied this strategy for the detection of thrombin. As shown in Fig. 17, ss-DNA-AuNP conjugates were hybridized with the aptamer to generate a separation length of ca. 12 nm between CdS nanocrystal and Au NPs. The system showed 5-fold enhancement in ECL intensity as compared to that without AuNPs, which might be attributed to the surface plasmon resonance field of AuNP. Later, Deng et al. (2014) have reported an ECL enhancement due to the interactions of the excited CdS: Eu nanocrystals with ECL-induced SPR in AuNPs at large separation distance. This system showed a 7.4-fold enhancement in the ECL intensity, and provided great sensitivity for the detection of thrombin with wide detection range from 50 aM to 1pM. Recently, Wang et al. (2016a) have demonstrated a different approach, based on the near-infrared ECL *resonance energy transfer (RET)* between CdTe/CdS QDs (as a donor) and gold nanorods (as acceptor). Gold nanorods were assembled onto CdTe/CdS film by DNA hybridization between aptamers and their css-DNA. In the absence of thrombin, the near-infrared ECL of QDs was quenched as a result of the ECL-RET of QDs to gold nanorods. In the presence of

thrombin, the near-infrared ECL of the system was "turned on" because thrombin can replace the gold nanorods onto the QDs film, owing to the specific aptamer-protein affinity interactions. Such approach gave a possibility to reach extremely low LoD for thrombin (=31 aM). The highly effective ECL-RET could be attributed not only to their appropriate separation distance but also to their overlapping emission/absorption spectra.

Both proposed SPR- and RET-based strategies were based on the "sandwich" assay format. Therefore, such strategies are suitable for the detection of large molecules. It demonstrates advantages in the form of sensitive and controllable ECL switches for signal amplification.

4 Signal amplification strategies in ECL aptasensors assays

4.1 Nanomaterials-based amplification of the ECL efficiency

As a fundamental and crucial element, amplification is in continuous demand to permit the highest sensitivity. Generally ECL aptasensors have been classified into two classes according to the amplification strategies. The first one is *nanomaterials-based amplification*, which have attracted widespread attention in ECL aptasensors. Tables 1-3 clearly displayed the diversity of nanomaterials and their composites that have been utilized in ECL aptasensors as immobilization supports for loading abundant capture probes and ECL probes, as well as excellent carriers in the transduction amplification of recognition events. From the above tables, it can be concluded that the ECL aptasensors in combination with nanomaterials has possessed significantly higher sensitivity and wide detection range in comparison with aptasensors without employing nanomaterials. For example, CdSe QDs can adsorb more aptamers with the help of carboxyl and the amino groups to improve the

ECL-signal (Li et al., 2012). Chen et al. (2010) has demonstrated that the application of $Ru(bpy)_3^{2+}$-doped silica NPs achieved more than 1000-fold enhancement of the ECL signals in comparison with single $Ru(bpy)_3^{2+}$ molecules. Zhang et al. (2013) have reported that the ECL intensity of the ZnO@carbon QDs nanostructure in 0.01 M phosphate buffer solutions (pH7.4) containing 0.01 M $K_2S_2O_8$ and 0.01 M KCl was 4-fold higher than the pure carbon QDs and 9-fold higher than the pure ZnO nanosphere. This indicates that the high surface-to-volume ratio of ZnO is beneficial for high loading of carbon QDs and such conjugate can be used as good ECL label for ECL aptasensor.

4.2 Isothermal nucleic acid-based amplification of the ECL efficiency

Nucleic acid amplification is one of the most valuable tools in nucleic acid detection, as it can significantly improve the sensitivity of the assay. The *polymerase chain reaction* (PCR) has become an indispensable tool in numerous molecular research and diagnostic applications. However, this strategy has some disadvantages because of the intrinsic property of PCR, such as high-precision temperature cycling, nonspecific, sophisticated equipment requirements and time-consuming analysis for PCR products.

Mirkin and coworkers have developed a NPs-based biobarcode technique (Nam et al. 2003) that provides PCR-like sensitivity for protein detection without applying enzymatic amplification. This strategy has also been successfully employed for signal amplification in ECL aptasensors. The typical ECL biobarcode involves two types of particles (Zhou et al., 2012) including a *magnetic microparticle* (usually streptavidin-coated) with recognition elements (aptamer) covalently attached to its surface, and an *AuNP* that has linked to another aptamer (thiol labeled), which can form a sandwich structure around the target in conjunction with the magnetic particle.

Also, hundreds of thiolated DNA and ECL-tags (*bio-barcoded nanoprobe*) can be strongly bound at gold surface through Au-thiol binding. The two types of particles have been incubated with the target to form the sandwich structures, whereas a magnetic field is used to localize and collect them. After the excess Au-NPs have been removed, the barcode strands release from the AuNPs through ligand exchange. The thousands of barcodes on each AuNPs amplified the signal, making it possible to detect vanishingly small quantities of their target protein.

Duan and Zhou et al. (2012) have described the ECL biobarcode assay by employing *cysteamine – AuNP* conjugates instead of double labeling oligonucleotides. This assay allows the identification of thrombin down to 1 pM concentration on a timescale of 1 hour with the dynamic range covers 4 orders of magnitude (Fig.18). Later, Chen et al. (2014b) developed an ECL platform based on bio-barcode amplification strategy in combination with *rolling circle amplification* (RCA) for the sensitive (16 cell mL^{-1}) detection of Ramos Cells.

It is important to mention that the well-defined magnetic collection of the aptamer-target protein-ECL nanoprobe complexes on the electrode surface should ensure the high reproducibility of assay. Moreover, the direct detection of ECL signals without immobilization and repeated hybridization of biobarcodes may also improve the reproducibility as well as the sensitivity of the method.

To date, several ECL aptamer-based methods have been designed in combination with isothermal amplification techniques, such as *loop mediated isothermal amplification* (Yuan et al., 2014b), *exonclease-catalyzed target recycling amplification* (Wu et al., 2015, Yang et al., 2014), *rolling circle amplification* (Chen et al. 2014b), and *hyper branched rolling circle amplification* (Jin et al., 2015). For example, Jin et al. (2015) proposed an aptasensor strategy by taking advantage of the

higher amplification efficiency of hyper branched rolling circle amplification to achieve the highly sensitive and specific detection of thrombin up to 1.2 aM, which is superior to the previously reported methods (for the comparison, please see Table 3). The isothermal amplification has advantages of extremely fast amplification and didn't require thermo-cyclers.

Recently, *DNAzymes* have attracted research interests to construct ECL aptasensors (Xia et al., 2015; Shi et al. 2014; Zhao et al., 2015) due to their low cost, easy to label, and more stable nature against hydrolysis and heat treatment. For instance, Xia et al. (2015) introduced amplification strategies based on both biobar coded Au NPs for QDs enrichment and DNAzyme recycling into single ECL system in order to develop an ideal sensing platform for the protein detection. Thus the excellent sensitivity with the LoD of 0.28 fM and linear range over 3 orders of magnitude was achieved for the detection of thrombin. Shi et al. (2015) constructed an ECL aptasensor based on the CdS-MoS_2 as ECL luminescence reagent and DNAzyme as ECL quencher for the detection of immunoglobulin E. Zhao et al. (2015) provided the "switch off" state of ECL aptasensor by utilizing the quenching effect of hemin/G-quadruplex DNAzymes towards $S_2O_8^{2-}$-O_2 system. The DNA hybridization reaction of assistant probes (guanine-rich nucleic acid) with capture probes can generate a large amount of hemin/G-quadruplex DNAzymes in the presence of hemin with a simple and label-free process. Thus, this strategy resulted in an excellent linear response (0.15 nM to 170 mM), as well as sensitivity (LoD = 45 pM) for kanamycin detection. *Exonuclease-assisted cycling ECL signal amplification* has been reported by Zhang et al. (2015) in quadruplex DNAzyme-based ECL biosensing strategy for the detection of vascular endothelial growth factor with LoD of 0.2pM. It can be concluded that the

combination of the isothermal amplification and ECL aptsensors platforms proved a valuable detection strategy to achieve high sensitivity in PCR-based methods.

Conclusions and Future Perspectives

In recent decades, the wide interest of the researcher community in ECL aptasensors with various detection strategies for a wide range of analytes has been convincingly documented. Many unique properties of aptamers, such as the capability of structure switching, hybridization with css-DNA, adsorption onto carbon materials, and nucleic acid amplification, as well as susceptibility to the action of a specific type of enzyme, have been utilized for the development of the different proof-of-concepts in ECL aptasensors platforms. The basic of widespread ECL concepts, such as nanomaterials-enhanced ECL, surface plasmon and RET coupled ECL, bipolar electrode coupled ECL, as well as the quenching of ECL, have been adapted in aptasensors platform. Different types of targets, such as proteins, toxins, live cells, heavy metals and other clinically relevant molecules, have been determined with the high sensitivity.

Since the binding affinity of aptamers is highly influenced by the ionic condition, temperature, and pH of the binding medium, challenges remain in eliminating cross-binding activities to other molecules in native environments. Thus, the future improvement of ECL aptasensors performance strongly depends on a progress in SELEX methodology for the selection of high affinity aptamers, the optimization of the immobilization strategy (both of ssDNA, and detection probe), as well as working parameters of the whole system. Currently, POCT for different diseases is quite common. One of the main constraints of the POCT is low sensitivity. The development of POCT based on ECL aptasensor, which combine the high sensitivity

of ECL, the diversity of aptamer target molecules and the portability of detection, will facilitate the development of more sensitive and widely used POCT technologies. With the successful selection of more apatamers, the application of ECL aptasensors for high throughput analysis and multiplex analysis will receive increasing attention. In view of the broad applications of both ECL and aptasensors, ECL aptasensors undoubtedly will receive much attention.

Acknowledgment

This project was kindly supported by The National Key Research and Development Program of China (No. 2016YFA0201300), the National Natural Science Foundation of China (Nos. 21475123 and 21505128), the CAS President's International Fellowship Initiative (PIFI) project, and the Chinese Academy of Sciences (CAS)–the Academy of Sciences for the Developing World (TWAS) President's Fellowship Programme (2013-053).

References

Bard, A.J., 2004. 1. Introduction, in: Bard, A.J. (Ed.), Electrogenerated Chemiluminescense. Marcel Dekker, New York, pp. 1-22.

Bouffier, L., Arbault, S., Kuhn, A. et al. 2016. Anal. Bioanal. Chem. 408, 7003-7011.

Bruno, J.G., Richarte, A.M., Phillips, T., 2014. Microchem. J. 115, 32-38.

Bu, N., Gao, A., He, X., Yin, X., 2013. Biosens. Bioelectron., 43, 200-204.

Cai, Q., Chen, L., Luo, F., Qiu, B., Lin, Z., Chen, G., 2011. Anal. Bioanal. Chem. 400 (1), 289-294.

Cao, J., Wang, H., Liu, Y., 2015. Spectrochim. Acta Part A: Mol. and Biomol. Spectrosc. 151, 274-279.

Cao, W., Ferrance, J.P., Demas, J., Landers, J.P., 2006. J. Am. Chem. Soc. 128(23), 7572-7578.

Chai, Y., Tian, D., Gu, J., Cui, H, 2011. Analyst 136(16), 3244-3251.

Chen, A., Yan, M., Yang, S., 2016a. TrAC, Trends Anal. Chem., 80, 581-593.

Chen, A., Yang, S., 2015a. Biosens. Bioelectron., 71, 230-242.

Chen, H., Chen, Q., Zhao, Y., Zhang, F., Yang, F., Tang, J., He, P., 2014a. Talanta 121, 229-233.

Chen, H., Huang, J., Palaniappan, A., Wang, Y., Liedberg, B., Platt, M., Tok, A.I.Y., 2016b. Analyst 141(8), 2335-2346.

Chen, L., Cai, Q., Luo, F., Chen, X., Zhu, X., Qiu, B., Lin, Z., Chen, G., 2010. Chem. Commun., 46(41), 7751-7753.

Chen, L., Zeng, X., Ferhan, A. R., Chi, Y., Kim, D., Chen, G., 2015b. Chem. Commun., 51(6), 1035-1038.

Chen, M., Bi, S., Jia, X., He, P., 2014b. Anal. Chim. Acta 837, 44-51.

Chen, Q., Chen, H., Zhao, Y., Zhang, F., Yang, F., Tang, J., He, P., 2014c. Biosens. Bioelectron., 54, 547-552.

Chen, Y., Jiang, B., Xiang, Y., Chai, Y., Yuan, R., 2011. Chem. Commun., 47(27), 7758-7760.

Deng, L., Du, Y., Xu, J., Chen, H., 2014. Biosens. Bioelectron., 59, 58-63.

Ding, C., Zheng, Q., Wang, N., Yue, Q., 2012. Anal. Chim. Acta 756, 73-78.

Duan, R., Zhou, X., 2012. Progress in Biomedical Optics and Imaging - Proceedings of SPIE.

Ellington, A.D., Szostak. J.W., 1990. Nature 346, 818-822.

Feng, X., Gan, N., Lin, S., Li, T., Cao, Y., Hu, F., Chen, Y., 2016. Sens. Actuators, B: Chem., 226, 305-311.

Feng, X., Gan, N., Zhang, H., Yan, Q., Li, T., Cao, Y., Hu, F., Yu, H., Jiang, Q., 2015. Biosens. Bioelectron., 215, 587-593.

Forster, R.J., Keyes, T.E., 2013. Electrochemiluminescent Biosensors: Neuroscience Applications, in: Marinesco S., Dale, N. (Eds.), Microelectrode Biosensors. Humana press, New York, pp. 347-369.

Gan, X., Yuan, R., Chai, Y., Yuan, Y., Cao, Y., Liao, Y., Liu, H., 2012a. Anal. Chim. Acta 726, 67-72.

Gan, X., Yuan, R., Chai, Y., Yuan, Y., Mao, L., Cao, Y., Liao, Y., 2012b. Biosens. Bioelectron., 34(1), 25-29.

Germain, R. 1986. Nature 322, 687-689.

Gui, G., Zhuo, Y., Chai, Y., Liao, N., Zhao, M., Han, J., Xiang, Y., 2013. Biosens. Bioelectron., 47, 524-529.

Gui, G., Zhuo, Y., Chai, Y., Liao, N., Zhao, M., Han, J., Yuan, R, 2014. RSC Adv., 4(4), 1955-1960.

Gui, G.-., Zhuo, Y., Chai, Y., Xiang, Y., Yuan, R., 2016. Biosens. Bioelectron., 77, 7-12.

Guo, X., Wu, S., Duan, N., Wang, Z., 2016. Anal. Bioanal. Chem., 408(14), 3823-3831.

Hai, H., Yang, F., Li, J., 2013. RSC Adv., 3(32), 13144-13148.

He, Y., Chai, Y., Wang, H., Bai, L., Yuan, R., 2014. RSC Adv., 4(100), 56756-56761.

Holmberg, A., Blomstergren, A., Nord, O., Lukacs, M., Lundeberg, J., Uhlén, M. 2005. Electrophoresis 26 (3), 501-510.

Hong, L., Chai, Y., Zhao, M., Liao, N., Yuan, R., Zhuo, Y., 2015a. Biosens. Bioelectron., 63, 392-398.

Hong, L., Wang, J., Zhuo, Y., Chai, Y., Zhao, M., Gui, G., Yuan, R., 2015b. Electrochim. Acta 186, 174-181.

Hu, L., Bian, Z., Li, H., Han, S., Yuan, Y., Gao, L., Xu, G., 2009. Anal. Chem., 81(23), 9807-9811.

Huang, H., Tan, Y., Shi, J., Liang, G., Zhu, J.-J., 2010. Nanoscale 2(4), 606-612.

Huang, H., Zhu, J.-J., 2009. Biosens. Bioelectron., 25(4), 927-930.

Huang, X., Li, Y., Zhang, X., Zhang, X., Chen, Y., Gao, W., 2015. Analyst 140(17), 6015-6024.

Jarczewska, M., Gorski, L., Malinowska, E., 2016. Anal. Methods 8(19), 3861-3877.

Jin, G., Lu, L., Gao, X., Li, M., Qiu, B., Lin, Z., Chen, G., 2013. Electrochim. Acta 89, 13-17.

Jin, G., Wang, C., Yang, L., Li, X., Guo, L., Qiu, B., Chen, G., 2015. Biosens. Bioelectron., 63, 166-171.

Kong, Q., Li, M., Ma, C., Yang, H., Ge, S., Yan, M., Yu, J. 2015. RSC Adv., 5, 70345-70351.

Kong, Q., Li, M., Ma, C., Yang, H., Ge, S., Yan, M., Yu, J., 2015. RSC Adv., 5(86), 70345-70351.

Lei, Y., Huang, W., Zhao, M., Chai, Y., Yuan, R., Zhuo, Y., 2015. Anal. Chem., 87(15), 7787-7794.

Li, F., Cui, H., 2013. Biosens. Bioelectron., 39(1), 261-267.

Li, G., Yu, X., Liu, D., Liu, X., Li, F., Cui, H., 2015. Anal. Chem., 87(21), 10976-10981.

Li, M., Yang, H., Ma, C., Zhang, Y., Ge, S., Yu, J., Yan, M., 2014. Sens. Actuators B: Chem., 191, 377-383.

Li, Y., Liu, L., Fang, X., Bao, J., Han, M., Dai, Z., 2012. Electrochim. Acta 65, 1-6.

Li, Y., Qi, H., Gao, Q., Zhang, C., 2011. Biosens. Bioelectron., 26(5), 2733-2736.

Li, Z., Qi, H., Yang, H., Gao, Q., Zhang, C., 2014a. Anal. Methods 6(5), 1317-1323.

Li, Z., Sun, L., Zhao, Y., Yang, L., Qi, H., Gao, Q., Zhang, C., 2014b. Talanta 130, 370-376.

Liao, Y., Yuan, R., Chai, Y., Mao, L., Zhuo, Y., Yuan, Y., Bai, L., Yuan, S., 2011a. Sens. Actuators B: Chem., 158(1), 393-399.

Liao, Y., Yuan, R., Chai, Y., Zhuo, Y., Yuan, Y., Bai, L., Yuan, S., 2011b. Biosens. Bioelectron., 26(12), 4815-4818.

Lin, Z., Chen, L., Zhu, X., Qiu, B., Chen, G., 2010. Chem. Commun., 46(30), 5563-5565.

Liu, D., Xin, Y., He, X., Yin, X., 2011. Analyst 136(3), 479-485.

Liu, W., Yang, H., Ge, S., Shen, L., Yu, J., Yan, M., Huang, J., 2015a. Sens. Actuators, B: Chem., 209, 32-39.

Liu, Y., Shi, G., Zhang, J., Zhou, M., Cao, J., Huang, K., Ren, S., 2014a. Colloids and Surfaces B: Biointerfaces 122, 287-293.

Liu, Y., Zhang, J., Shi, G., Zhou, M., Liu, Y., Huang, K., Chen, Y., 2014b. Electrochim. Acta 129, 222-228.

Liu, Y., Zhou, M., Liu, Y., Huang, K., Cao, J., Zhang, J., Chen, Y., 2014c. Anal. Methods 6(12), 4152-4157.

Liu, Y., Zhou, M., Liu, Y., Shi, G., Zhang, J., Cao, J., Chen, Y., 2014d. RSC Adv., 4(44), 22888-22893.

Liu, Y., Zhou, M., Liu, Y., Shi, G., Zhang, J., Cao, J., Chen, Y., 2014. RSC Adv., 4, 22888-22893.

Liu, Y.-M., Yang, J.-J., Cao, J.-T., Zhang, J.-J., Chen, Y.-H., Ren, S.-W., 2016. Sens. Actuators B: Chem., 232, 538-544.

Liu, Z., Qi, W., Xu, G., 2015. Chem. Soc. Rev. 44, 3117-3142.

Liu, Z., Zhang, W., Hu, L., Li, H., Zhu, S., Xu, G, 2010. Chem. - A Europ. J., 16(45), 13356-13359.

Liu, Z., Zhang, W., Qi, W., Gao, W., Hanif, S., Saqib, M., Xu, G., 2015b. Chem. Commun., 51(20), 4256-4258.

Lu, J., Yan, M., Ge, L., Ge, S., Wang, S., Yan, J., Yu, J., 2013. Biosens. Bioelectron., 47, 271-277.

Ma, F., Jia, L., Zhang, Y., Sun, B., Qi, H., Gao, Q., Zhang, C., 2011. Sci. China Chem. 54(8), 1357-1364.

Ma, M., Zhang, X., Zhuo, Y., Chai, Y., Yuan, R., 2015. Nanoscale 7, 2085-2092.

Ma, M., Zhang, X., Zhuo, Y., Chai, Y., Yuan, R., 2015a. Nanoscale 7(5), 2085-2092.

Ma, M., Zhuo, Y., Yuan, R., Chai, Y., 2015b. Anal. Chem., 87(22), 11389-11397.

Muzyka, K., 2014. Biosens. Bioelectron., 54, 393–407.

Nam, J.-M., Thaxton, C.S., Mirkin, C.A. 2003 Science 301, 1884−1886.

Piran, U., Riordan, W.J., 1990. J. Immunol. Methods 133, 141–143.

Ravalli, A., Voccia, D., Palchetti I.and Marrazza G. Biosensors 2016, 6, 39.

Ruscito, A., DeRosa, M.C., 2016. Front. Chem. 4 (14) (in press).

S. Vigneshvar, C.C.S., B. Senthilkumaran, and H. Prakash, 2016. Frontiers in Bioengn. Biotechn. 4(11).

Sharma, S.B., Hannah; O'Kennedy, Richard J., 2016. Essays in biochem., 60(1), 9-18.

Shi, G., Cao, J., Zhang, J., Huang, K., Liu, Y., Chen, Y., Ren, S., 2014a. Analyst 139(22), 5827-5834.

Shi, G., Cao, J., Zhang, J., Liu, Y., Chen, Y., Ren, S., 2015. Sens. Actuators, B: Chem., 220, 340-346.

Shi, H.-W., Wu, M.-S., Du, Y., Xu, J.-J., Chen, H.-Y., Shi, H.-W., Wu, M.-S., Du, Y., Xu, J.-J., Chen, H.-Y., 2014b. Biosens. Bioelectron., 55, 459-463.

Simonsson, T., 2001. Biological Chemistry 382(4), 621–628.

Stojanovic, M. N., de Prada, P., Landry, D. W., 2000. J. Am. Chem. Soc 122(46), 11547–11548.

Su, M., Liu, H., Ge, L., Wang, Y., Ge, S., Yu, J., Yan, M., 2014. Electrochim. Acta 146, 262-269.

Sun, H., Zu, Y., 2015. Molecules 20(7), 11959-11980.

Swathi, R.S., Sebastian, K.L. (2009) J. Chem. Phys. 130, 86-101.

Tang, X., Zhao, D., Zhang, M., 2013. Analyst 138(19), 5706-5712.

Tuerk, C., Gold L., 1990. Sci. China Chem. 249, 505-510.

Tyagi, S., Kramer F.R., 1996. Nature Biotechn. 14, 303–308.

Wang, C., Qian, J., Wang, K., Hua, M., Liu, Q., Hao, N., Huang, X., 2015. ACS Appl. Mat. Interfaces 7(48), 26865-26873.

Wang, H., Gong, W., Tan, Z., Yin, X., Wang, L., 2012. Electrochim. Acta 76, 416-423.

Wang, J., Jiang, X., Han, H., 2016a. Biosens. Bioelectron., 82, 26-31.

Wang, J., Shan, Y., Zhao, W., Xu, J., Chen, H., 2011. Anal. Chem., 83(11), 4004-4011.

Wang, X., Dong, P., He, P., Fang, Y., 2010. Anal. Chim. Acta 658(2), 128-132.

Wang, X., Dong, P., Yun, W., Xu, Y., He, P., Fang, Y., 2009. Biosens. Bioelectron., 24(11), 3288-3292.

Wang, X., Gao, A., Lu, C., He, X., Yin, X., 2013. Biosens. Bioelectron., 48, 120-125.

Wang, X., Yun, W., Zhou, J., Dong, P., He, P., Fang, Y., 2008. Chinese J. Chem. 26(2), 315-320.

Wang, X., Zhou, J., Yun, W., Xiao, S., Chang, Z., He, P., Fang, Y., 2007. Anal. Chim. Acta 598(2), 242-248.

Wang, Y.-Z., Hao, N., Feng, Q.-M., Shi, H.-W., Xu, J.-J., Chen, H.-Y., 2016b. Biosens. Bioelectron., 77, 76-82.

Wei, X.-P., Yang, F., Ding, F., Li, J.-P., 2014. Chinese J. of Anal. Chem., 42(7), 942-947.

Witt, M., Walter, J.-G., Stahl, F., 2015. Microarrays 4, 115-132.

Wu, D., Xin, X., Pang, X., Pietraszkiewicz, M., Hozyst, R., Sun, X., Wei, Q., 2015. ACS Appl. Mat. Interfaces 7(23), 12663-12670.

Xia, H., Li, L., Yin, Z., Hou, X., Zhu, J., 2015. ACS Appl. Mat. Interfaces 7(1), 696-703.

Xiao, L., Chai, Y., Yuan, R., Wang, H., Bai, L., 2014. Analyst 139(5), 1030-1036.

Yan, J., Yan, M., Ge, L., Yu, J., Ge, S., Huang, J., 2013. Chem. Commun., 1383-1385.

Yang, L., Zhu, J., Xu, Y., Yun, W., Zhang, R., He, P., Fang, Y., 2011. Electroanalysis 23(4), 1007-1012.

Yang, M., Jiang, B., Xie, J., Xiang, Y., Yuan, R., Chai, Y., 2014. Talanta 125, 45-50.

Yao, W., Wang, L., Wang, H., Zhang, X., Li, L., 2009. Biosens. Bioelectron., 24(11), 3269-3274.

Yin, X.-B., 2012. TrAC, Trends Anal. Chem., 33, 81-94.

Yin, X.-B., Xin, Y.-Y., Zhao, Y., 2009. Anal. Chem., 81(22), 9299-9305.

Yu, F., Li, G., Mao, C., 2011. Electrochem. Com. 13(11), 1244-1247.

Yu, Y., Cao, Q., Zhou, M., Cui, H., 2013. Biosens. Bioelectron., 43(1), 137-142.

Yuan, T., Liu, Z.-Y., Hu, L.-Z., Xu, G.-B., 2011. Chinese J. of Anal. Chem., 39(7), 972-977.

Yuan, Y., Gan, X., Chai, Y., Yuan, R., 2014a. Biosens. Bioelectron., 55, 313-317.

Yuan, Y., Wei, S., Liu, G., Xie, S., Chai, Y., Yuan, R., 2014b. Anal. Chim. Acta 811, 70-75.

Zhang, H., Li, M., Li, C., Guo, Z., Dong, H., Wu, P., Cai, C., 2015. Biosens. Bioelectron., 74, 98-103.

Zhang, J., Cao, J., Shi, G., Huang, K., Liu, Y., Chen, Y., 2014. Anal. Methods 6(17), 6796-6801.

Zhang, J., Cao, J., Shi, G., Huang, K., Liu, Y., Ren, S., 2015a. Talanta 132, 65-71.

Zhang, J., Cao, J., Shi, G., Liu, Y., Chen, Y., Ren, S., 2015b. Talanta 141, 158-163.

Zhang, J., Chen, J.H., Chen, R.C., Chen, G.N., Fu, F.F. 2009. Biosens. Bioelectron., 25, 815–819.

Zhang, J., Chen, P., Wu, X., Chen, J., Xu, L., Chen, G., Fu, F., 2011. Biosens. Bioelectron., 26(5), 2645-2650.

Zhang, M., Liu, H., Chen, L., Yan, M., Ge, L., Ge, S., Yu, J., 2013. Biosens. Bioelectron., 49, 79-85.

Zhao, M., Zhuo, Y., Chai, Y., Yuan, R., 2015. Biomaterials 52(1), 476-483.

Zhao, T., Lin, C., Yao, Q., Chen, X., 2016. Talanta 154, 492-497.

Zhao, Y., He, X., Yin, X., 2011. Chem. Commun., 47(22), 6419-6421

Zhou, X., Duan, R., Xing, D., 2012. Analyst 137(8), 1963-1969.

Zhu, D., Zhou, X., Xing, D., 2010. Biosens. Bioelectron., 26(1), 285-288.

Zhu, D., Zhou, X., Xing, D., 2012. Anal. Chim. Acta 725, 39-43.

Zhuo, Y., Ma, M., Chai, Y., Zhao, M., Yuan, R., 2014. Anal. Chim. Acta 803, 47-53.

Figure and Table Captions:

Fig. 1. Schematic representation of sandwich assay format (aptamer I as a capture probe, aptamer II as a reported probe) directed against the target molecule of interest

Fig. 2. Schematic representation of structure and switching principle of a labeled MBA with an ECL reporter and quencher

Fig. 3. Illustration of ECL sensing platforms based on change of quenching effect via target induced structure-switching of Fc-labeled MBA. Adapted from reference (Wang et al., 2009) with modifications

Fig. 4. Illustration of "Signal on" ECL strategy based on target-induced displacement of Fc-labeled aptamer. Adapted from reference (Chen et al., 2010) with modifications

Fig. 5. Illustration of "Signal off" ECL strategy based on target induced css-DNA displacement and structure switching of quencher-labeled aptamer. Adapted from reference (Wang et al. (2010)) with modifications

Fig. 6. Illustration of "Signal off" ECL strategy based on target-induced displacement of Fc-labeled aptamer coupled with a bipolar electrode concept. Adapted from reference (Shi et al., 2014) with modifications

Fig. 7. Illustration of "Signal on" strategy based on target induced desorption of ECL-tag-labeled aptamer from GO. Adapted from reference (Huang et al., 2015) with modifications

Fig. 8. Illustration of "Signal off" strategy based on target induced desorption of ECL-tag-labeled aptamer from the SWCNT. Adapted from reference (Li et al., 2014a) with modifications

Fig. 9. Schematic representation of ECL sensing platforms based on the junction-probe strategy. Reprinted from reference (Zhang et al., 2011) with modifications

Fig. 10. Illustration of "Signal off" detection approach based on target induced displacement of the ECL-tag-labeled css-DNA. Adapted from reference Wang et al. (2007) with modifications

Fig. 11. Illustration of "Signal on" detection approach based on target induced displacement of the ECL-tag-labeled css-DNA. Adapted from reference (Yao et al. (2009)) with modifications

Fig. 12. Illustration of "Signal on" target induced strand displacement ECL label-strategy based on additional utilization of an auxiliary probe. Adapted from reference (Li et al., 2014b) with modifications

Fig. 13. Illustration of the label-free intercalation-based "Signal off" strategy of the ds-DNA-based ECL aptasensor. Adapted from reference (Yin et al., 2009)), with modifications.

Fig. 14. Illustration of the label-free intercalation-based "Signal off" strategy of the ts-DNA-based ECL aptasensor. Adapted from reference (Bu et al., 2013) with modifications.

Fig. 15. Illustration of the label-free intercalation-based "Signal on" strategy of the duplex-DNA-based ECL aptasensor. Adapted from reference (Zhao et al., 2011) with modifications

Fig. 16. "Signal on" principle of determination of Pb^{2+} ions based on G-quadruplex of aptamer probe. Adapted from reference (Wei et al., 2014), with modifications

Fig. 17. ECL aptamer sensing platform based on energy transfer between CdS nanocrystals and AuNPs. Reprinted from reference (Wang et al., 2011) with permission

Fig. 18. Schematic description of the ECL aptasensor for human thrombin and ATP based upon the amplification of biobarcode method. Reprinted from reference (Zhou et al., 2012)) with permission

Table 1 – Data on the performance of aptamer-based ECL assay for two-site binding (sandwich-type) configuration

Detection limit / working range	**ECL-reporter probe (aptamer II)**	**Matrix for immobilization of capture probe (aptamer I) / electrode**	**Notes**	**Ref**
Target analyte: THROMBIN (enzyme)				
0.03 fM / 0.1 fM to 1 nM	(AuNPs-semicarbazide)n-hollow Au nanocages + -NH_2-TBA II	BSA / SH-TBA I / AuNPs / CdTe QDs@C60NPs / **GCE**	Semicarbazide, as co-reaction accelerator. AuNPs enhance the ECL reaction rate of CdTe QDs and $S_2O_8^{2-}$	Ma et al., 2015 b
0.3 fM / 1 fM –10 nM	HAuNPs / GOxNPs / PtNPs / NH_2-TBA II	BSA / SH-TBA I / AuNP / C60 / **GCE**	Mimicking bi-enzyme nanocomplexes, as a signal enhancer	Zhuo et al., 2014
0.3 fM / 0.1 µM to 10 µM	Ppy-pa NPs / Ru1- NH_2 / TBA-II	NH_2-TBA-I / 4-aminobenzene sulfonic acid / **Paraffin-impregnated graphite electrode**	Graphite electrode covalently modified with a monolayer of 4-aminobenzene sulfonic acid => for thrombin capturing. Ppy-pa NPs, as a carrier of Ru1	Ma et al., 2011
0.33 fM / 1.0 fM to 1.0 pM	$[Ru(phen)_2(cpaphen)]^{2+}$ − ampicilin@CNTs−PEI−AuNCs− NH_2-TBA II	SH- TBA I / AuNPs / **Gr−Nf -modified electrode**	*In situ* generation of self-enhanced luminophore by β-Lactamase (ampicillin) catalysis. Immobilization of Ru−Ampiciline via π−π stacking interactions to form the Ru−Amp@CNTs nanocomposite	Gui et al., 2014
0.33 fM / 1 fM to 1 nM	Graphene sheets - 3,4,9,10-perylenetetracarboxylic dianhydride / NH_2-TBA II	TB / hexanethiol / SH- TBA I / $HAuCl_4$ / **Au-electrode**	Perylenetetracarboxylic dianhydride and GS => ↑ ECL of	Gan et al.,

			$S_2O_8^{2-}$ system	2012 a
0.54 fM / 1 fM to 10 pM	pNAMA-Ru2-HGNPs-NH_2-TBAII	1-hexanethiol / SH-TBAI / PEI@ dendriticAuNPs / CNTs–Nf / **GCE**	PEI, as a co-reactant of Ru2. Coating of electrode through electrostatic adsorption	Gui et al., 2016
1.0 fM 2.0 fM to 2.0 pM	Ru-doped SNPs / NH_2-TBA II	SH-TBA I / **Au electrode**	TPA, as co-reactant	Wang et al., 2008
1.3 fM / 0.02 to 5.0 pM	CdSe–ZnS QDs / NH_2 -TBA II	MCH / SH-TBA I / AuNPs / MoS_2–GR / **GCE**	MoS_2–GR composites => ↑ loading capacity and conductivity of the GCE. EDC and NHS – based conjugation of CdSe–ZnS QDs to TBA II	Liu et al., 2014 a
1.6 fM / 5 fM to 50 pM	$Ru(phen)_3^{2+}$-ds-DNA-streptavidin- HAuNPs – NH_2-TBA II	Hexanethiol / TBAI /Au@Pd/ GR–Nf / **GCE**	HAuNPs, as tag-carriers. Two single DNA strands of S2 and S3 for i*n situ* propagate a chain reaction of hybridization events to obtain ds-DNA. $Ru(phen)_3^{2+}$ intercalation into the grooves of ds-DNA	Gui et al., 2013
3 fM / 0.01 pM to 0.1 nM	TBA II / Ru-Poly(ethylenimine) - polyanion poly(acrylic acid)	BSA / multifunctional binding aptamer / PCS / nano-Au / thiosemicarbazide / AuNPs / **GCE**	PEI and thiosemicarbazide, as **dual co-reactants**	Hong et al., 2015 b
3.3 fM / 0.1µ to 10 nM	TBA II / AuNPs / 3,4,9,10-perylene tetracarboxylic acid-thiosemicarbazide / C60 NPs	SH-TBA 1 / AuNPs / Gr / **GCE**	Peroxydisulfate / oxygen ($S_2O_8^{2-}/O_2$) system	Ma, et al., 2015
5.0 fM / 0.01 pM to 10 nM	Proline and polyamidoamine / PtNPs Ru– prolidase–avidin-TBAII bioconjugate	MCH / SH-TBAI / AuNPs / Gr / **GCE**	*In situ* generated proline and polyamidoamine, as coreactants. PtNPs, as a carrier to load Ru	Yuan et al., 2014 a
33 fM / 0.1 pM to 50 nM	Gold nanorods / glucose dehydrogenase / hemin / G-quadruplex / TBA II	BSA / SH-TBA I / dep-Au / **GCE**	Triple-enzyme cascade catalysis amplification strategy	Xiao et al., 2014
2.72 nM / 27.2 nM to	Avidin-QD / TBA II-biotin	MCH / SH-TBAI / **Au electrode**	Target-induced deneration of a	Huan

545 nM			"G-quartet structure". QDs –based ECL in aqueous solution	g et al. 2009
0.03 pM / 0.1 pM – 10 n M	Hemin / NH_2-TBA II / $Au@CeO_2$	BSA / SH-TBA I / nano-Au / Ru–PEI / **GCE**	ECL quenching. Simultaneous immobilization of Ru and the co-reactant	Hong et al., 2015 a
0.35 pM / 0.5 pM to 800 pM	Polystyrene-$(CdTe)_2$ labels / TBA II	MCH / TBA I / AuNPs / **GCE**	Layer-by-layer assembly of CdTe QDs onto the surfaces of the polystyrene microbeads => ECL label with signal amplification.	Chen et al., 2011

Target analyte: PLATELET DERIVED GROWTH FACTOR (protein that regulates cell growth and division)

Detection limit / Linear range	**ECL-reporter probe (aptamer II)**	**Matrix for immobilization of capture probe (aptamer I) / electrode**	**Notes**	**Ref**
0.0011 pM 0.01 pM to 100 pM	CdSe–ZnS QDs / Apt2	MCH / Apt1 / MoS_2–AuNPs / **GCE**	MoS_2–AuNP composites => ↑ conductivity of GCE and ↑ immobilized amount of aptamer. $K_2S_2O_8$, as a coreactant	Liu et al., 2014
0.017 pM / 0.1 pM to 0.5 nM	Glucose oxidase / SH-Apt2 / AuNPs	BSA / NH_2-Apt1 / AuNPs-electrochemically reduced grapheme / **GCE**	*In situ* generation of H_2O_2 from reaction between glucose oxidase and glucose. The catalytic behavior of AuNPs to the ECL of the luminol–H_2O_2 system	Zhang et al., 2015 a
0.027 pM / 0.1 pM to 10 pM	ABEI-AuNPs / SH-Apt2	Biotin-Apt1 / streptavidin-AuNPs / **Au electrode**	ABEI is a more efficient ECL reagent than luminol when it is attached to biomolecules	Chai et al., 2011
0.13 pM / 0.5 pM to 1 nM	CdS QDs / Polyamidoamine / NH_2 - Apt2	BSA / NH_2-Apt1 / MWCNTs–chitosan film / **GCE**	MWCNTs–chitosan film => ↑ conductivity and ↑ surface for immobilization of aptamer. Polyamidoamine dendrimers => ↑ ECL of CdS	Zhang et al., 2015 b

1 pM / 1 pM to 10 nM	SH-TBR-bio bar code DNAs / AuNPs / SH-Apt2	Biotin-Apt1 / streptavidin magnetic beads / **Pt electrode**	Bio bar code signal amplification Immunomagnetic separation => ↓ time of ECL assay	Zhu et al., 2012
80 pM 0.1 to 1000 nM	**Ru4** / Apt2	Biotin-Apt1 / streptavidin magnetic beads / **Pt electrode**	Immunomagnetic separation => ↓ time of ECL assay; TPA, as a coreactant	Zhu et al., 2010
Target analyte: BRAIN NATRIURETIC PEPTIDE (cardiac biomarker of heart failure)				
pg*mL^{-1} in 50% human serum / No data	Streptavidin– TBR / Biotin-Apt2	Biotin-Apt1 / **streptavidin magnetic beads**	ELISA-like microplate assay screening for the highest affinity aptamers and cross-reactivity assessments	Bruno et al., 2014
Target analyte: CARCINOEMBRYONIC ANTIGEN (glycoprotein, tumor marker)				
25.3 fg*mL^{-1} / 0.1 pg*mL^{-1} to 20 ng*mL^{-1}	Auxiliary probe II / Manganese dioxide–graphene	Hexanethiol / NH_2-Auxiliary probe I-Apt-ds-DNA / Ru5–pendant-PHMWNT / Nf / **GCE**	Amino-terminated polyamidoamine encapsulated AuNPs. Manganese dioxide–grapheme, as a quencher	He et al., 2014
Target analyte: MCF-7 CANCER CELLS				
230 cell*mL^{-1} / 500 to 2 × 10^{7}cells*mL^{-1}	Aptamer-carbon QDs@ mesoporous silica nanoparticles	Canavalin A / 3D-GR@AuNPs / **GCE**	Multiple binding between Canavalin A and mannose or trimannoside => ↑ cell capture efficiency => ↑ sensitivity	Su e al., 2014

Table 2 – Data on the performance of aptamer-based ECL assay for single-site binding configuration in a sandwich-like manner (target-induced conjunction of split aptamer fragments)

Detection limit / working range	**ECL-reporter probe (aptamer II)**	**Matrix for immobilization of capture probe (aptamer I) / electrode**	**Notes**	**Ref**
Target analyte: ADENOSINE TRIPHOSPHATE (a nucleoside triphosphate, a small molecule used				

		in cells as a coenzyme)		
0.03 pM / 0.1 pM to 10 nM	Fc /ss-DNA2 /	$Ru(bpy)_3^{2+}$-doped silica-ss-DNA1 / NPG / **GCE**	N-succinimidyl-4-(N-maleimidomethyl)cyclohexane-1-carboxylate, as a linking agent; TPA, as a coreactant	Li et al., 2014a
0.037 pM / 0.1 pM to 50 nM	RGO / PtPd / ss-DNA2-NH_2	MCH / SH-ss-DNA1 / Ag dendrite / **ITO electrode**	*In situ* generate O_2, as a coreactant; RGO/PtPd enhanced catalytic performance; Ag dendrites => ↑ surface area for aptamer immobilization	Liu et al., 2015
0.1 pM / 0.5 pM to 20 nM	PNNs@CdS QDs / ss-DNA2	ss-DNA1 / Graphene/polyaniline / **GCE**	CdS QDs and PNNs@CdS QDs labeles could react with $S_2O_8^{2-}$ => ↑ ECL signal	Kong et al., 2015
0.1 pM / 0.5 pM–7.0 nM	P-acid–Pt–Ag ANPs / ss-DNA2	ss-DNA1 / **porous Au-paper working electrode**	Microfluidic origami ECL device. P-acid–Pt–Ag ANPs as hollow porous nanostructures multi-ECL labels for ECL signals amplification	Yan et al., 2013
1.5 pM / 5 pM to 5 nM	SiO_2 / Graphene QDs / NH_2-ss-DNA2	SH-ss-DNA1 / **Au electrode**	H_2O_2, as coreactant. Anodic ECL of blue-luminescent Graphene QDs	Lu et al., 2013
0.64 µM / 0.64 µM to 1.0 mM	$Ru(phen)_3^{2+}$ / part ds-DNA	SH-aptamer's part / **Au electrode**	A label-free sandwich-type ECL sensing system based on target-induced conjunction of split aptamer fragments and $Ru(phen)_3^{2+}$ intercalation	Liu et al., 2010
Target analyte: COCAINE (a small molecule, a powerful nervous system stimulant)				
3.7 pM / 1.0 nM to10 pM	RuSiNP-labeled / NH_2 – Apt2	MCH / SH-AptI / **Au electrode**	(Dibutylamino)ethanol, as a coreactant. The surface coverage of the Au electrode by the capture probe was about 5.5×10^{11} molecules/cm^2	Cai et al., 2011

Table 3 – Data on the performance of aptamer-based ECL assay in single-site binding configuration

Detection limit / working range	**ECL sensing platform**	**Notes**	**Ref**
	LARGE MOLECULES		
	Target analyte: THROMBIN (enzyme)		
1.2 aM / 3.0 to 300 aM	Ru(phen)$_3^{2+}$ / ds-DNA (-SH-css-DNA hybridized with TBA) / **Au electrode** TPA (a co-reactant)	***Label free*.** Target induced HRCA => ↑ number of ds-DNA producing on the electrode surface => Ru(phen)$_3^{2+}$ intercalate in ds-DNA => **Signal on**	Jin et al., 2015
31aM / 100 aM to 10 fM	Aptamer CdTe / CdS core small/shell thick QDs / **GCE** hybridized with css-DNA-AuNRs	***Labeled css-DNA.*** Target induced displacement of the labeled css-DNA => ↓ quenching of ECL => **Signal on** The CdTe/ CdS QDs film at GCE showed stable ECL at 707 nm at ca.-1.45V. ECL-RET-based quenching of AuNRs ECL	Wang et al., 2016
0.28 fM / 1 fM to 1 nM	Biobar coded Au NPs-QDs / CdSeTe@ZnS QDs / capture DNA / **Au electrode**	***Labeled.*** Dual biobar-coded Au NPs-QDs and DNAzyme amplification strategies	Xia et al., 2015
0.33 fM / 1 fM to 10 nM	HT / TBA / SA–alkaine phosphatase conjugate / Ru–PtNPs / Nf / **GCE.** *in-situ* produced ascorbic acid (a co-reactant)	***Label-free***. Target induced blocking of ECL probe-modified electrode => **Signal off**	Liao et al. 2011b
2.0 fM / 5 fM to 5.0 pM	Ru(bpy)$_2$(mcbpy-O-Su-ester)(PF$_6$)$_2$ - auxiliary probe / **Au-electorde** TPA (a co-reactant)	***Labeled auxiliary probe.*** Target induced hybridization of ECL probe with the auxiliary probe => Ru-complex closer to the electrode surface => **Signal on**	Li et al., 2014b
3.6 fM /	BSA / SH-TBA / AuNPs / Ru / Nafion	***Label-free***. Target induced	Liu et

10 fM to 5.0 nM	/ MoS_2 –graphene / **GCE** TPA (a co-reactant)	blocking of ECL probe-modified electrode => **Signal off**	al., 2014 c
8 fM / 0.05 to 100 pM	Capture probe / Ru–AuNPs / **GCE**	***Labeled probe.*** Target induced reattaching of Fc-labeled probe from the "Y" junction (capture + aptamer + Fc-labeled probes) => ↓ quenching of ECL in Ru-AuNPs film => **Signal on**	Zhang et al., 2011
17 fM / 0.05 to 50 pM	d(A5-T5-ds-DNA thrombin)-$Ru(phen)_3^{2+}$ / **Au electrode** TPA (a co-reactant)	***Label-free***. Target induced dissociation of ds-DNA => extrication of intercalated $Ru(phen)_3^{2+}$ into the solution=> **Signal off** d(Am-Tn) as anchor linker offers several combined advantages (wider electrochemical window, can stand repetitious scanning) compared with conventional DNA-SH	Tang et al., 2013
50 fM / 0.1 pM to 100pM	Fc-MBA–$Ru(bpy)_3^{2+}$–AuNPs electrode / **Au electrode** TPA (a co-reactant)	***Labeled***. Target induced structure-switching of Fc-labeled MBA => ↓ quenching of ECL in substrate => **Signal on.**	Wang et al., 2009
50 fM / 0.1 pM to 1.0 nM	CTS-CdS QDs / Aligned carbon nanotubes / **GCE** $K_2S_2O_8$ (a co-reactant)	***Label-free***. Target induced blocking of ECL probe-modified electrode => **Signal off**	Yang et al. 2011
0.02 pM / 0.05 to 50 pM	$Ru(phen)_3^{2+}$-ds-DNA (css-DNA hybridized with TBA) / **Au electrode** TPA (coreactant)	***Label-free***. Target induced dissociation of ds-DNA => extrication of intercalated $Ru(phen)_3^{2+}$ into the solution => **Signal off**	Yin et al., 2009
0.1 pM / 10 nM to 1pM	Tris(bpyRu)- β-cyclodextrin / thrombin / NH_2-TBA / **GCE** DBAE (a co-reactant)	***Label-free***. Target induced restricting the host–guest recognition between tris(bpyRu)-β-CD and the aptamer => ↓ tris(bpyRu)-β-CD on the surface of the GCE => ***Signal off***	Chen et al. 2014c

0.2 pM / 0.33 pM to 33 pM	Ru- SiNPs / detection probe of aptamer split with capure probe of aptamer / **Au electrode**	***Labeled***. Target induced formation of G-quadruplex structure => ECL reagent attaching to the surface of the electrode => **Signal on**	Lin et al, 2010
0.22 pM / 1.0 pM to 1.0 nM	BSA / aptamer / AuNPs / Ru / Nf / Dopamine-melanin colloidal nanospheres / **GCE** TPA (a co-reactant)	***Label-free***. Target induced blocking of ECL probe-modified electrode =>**Signal off.**	Liu et al., 2014b
0.33 pM / 1.0 pM to 20 nM	HT / NH_2-TBA / HGNPs / $Ru(phen)_3^{2+}$@CNTs-Nf / **GCE**	***Label-free***. Target induced blocking of ECL probe-modified electrode => **Signal off**	Gui et al. 2014
0.4 pM / 0.001 to 30 nM	DMBA@PtNPsAptamer II hybridized with HT / Aptamer I / Ru–PtNPs / Nf@MWCNTs / **GCE** DMBA (a co-reactant)	***Labeled css-DNA.*** Target induced blocking of ECL probe-modified electrode via displacement of Aptamer II into the solution and the association of inert protein thrombin on the electrode surface => **Signal off**	Gan et al., 2012b
0.4 pM / 0.90 to 226 pM	NH_2-TBA hybridized with functional oligonucleotide / GO / **GCE** TPA (a co-reactant)	***Label-free.*** Target induced dissociation of ds-DNA => extrication of intercalated $Ru(phen)_3^{2+}$ into the solution => **Signal off**	Wang et al., 2013
1.7 pM / 5 pM to 50 nM	Fc-MBA / Ru-PtNPs / Nf / GS-CNTs / **GCE** TPA (a co-reactant)	***Labeled.*** Target induced structure-switching of Fc-labeled MBA => ↓ quenching effect in the ECL substrate => **Signal on**	Liao al. 2011a
1.7 pM / 0.005 to 50 nM	Luminol-AuNPs–probe 2 / TBA hybridized with AuNPs–probe1 / **Au electrode** H_2O_2 (a co-reactant)	***Label-free***. Target induced blocking of ECL probe-modified electrode => **Signal off**	Li and Qui, 2013
1.3 nM / 2.0 nM to 50 nM	Magnetic GO nanosheets / Ir(III) complex / NH_2- TBA DBAE (a co-reactant)	***Labeled.*** Target induced alteration of interactions between labeled aptamer and carbon materials => displacement of the aptamer from the GO surface => ↑ ECL in bulk solution => **Signal on**	Jin et al., 2013
No data / 0 to 64 g*mL^{-1}	NH_2-TBA / TGA-modified CdSe QDs / **ITO electrode**	***Label-free***. Target induced blocking of ECL probe-modified electrode => **Signal off**	Li et al., 2012

	$K_2S_2O_8$ (a co-reactant)		
Target analyte: LYSOZYME (enzymes that damage bacterial cell**)**			
0.45 pM / No data	SH-css-DNA hybridized with SH-aptamer / **Au electrode** TPA (a co-reactant)	***Label-free***. Target induced dissociation of ds-DNA => extrication of intercalated $Ru(phen)_3^{2+}$ into the solution => **Signal off** ds-DNA was able to preconcentrate TPA and acted as the acceptor of the protons released from protonated $TPAH^+$	Liu et al., 2011
0.12 nM / 0.64 nM to 0.64 µM	$Ru(bpy)_3^{2+}$ / SH-aptamer / **Au electrode** TPA (a co-reactant)	***Label-free***. Target induced dissociation of ds-DNA => extrication of intercalated $Ru(bpy)_3^{2+}$ into the solution => **Signal off**	Li et al., 2011
Target analyte: IMMUNOGLOBULIN E (antibody subclass)			
80 fM / 0.5 pM to 1.0 nM	BSA / SH-aptamer / AuNPs / CS / CdS / CS / **GCE** H_2O_2 (a co-reactant)	***Label-free***. Target induced blocking of ECL probe-modified electrode => **Signal off**	Cao et al. 2015
0.18 pM / 0.5 pM to 0.5 nM	Aptamer-AuNPs-HRP hybridized with NH_2-css-DNA / MoS_2-Poly (diallyldimethylammonium chloride)-CdSe/ZnS QDs / **GCE** $K_2S_2O_8$ (a co-reactant)	***Labeled***. Target induced releasing of HRP => ↓en zymes-stimulate biocatalytic precipitation reaction => ↓ amounts of insoluble products on the electrode => **Signal on**	Liu et al., 2016
0.34 pM / 0.001 to 10.0 nM	DNAzyme-AuNPs-aptamer hybridized with NH_2-css-DNA / CdS-MoS_2 **/ GCE** H_2O_2 (a co-reactant)	***Labeled***. DNAzyme electrocatalyze the reduction of H_2O_2 as the coreactant of CdS-MoS_2 ECL emission => ECL quenching => **Signal off**	Shi et al., 2015
Target analyte: CARCINOEMBRYONIC ANTIGEN (glycoprotein, tumor marker)			
3.8 $pg*mL^{-1}$ / 0.01 to 10.0 $ng*mL^{-1}$	BSA / SH-aptamer / AuNPs / L-cys / Nf / CdS–GR / **GCE** Peroxydisulfate ($S_2O_8^{2-}$) (a co-reactant)	***Label-free***. Target induced blocking of ECL probe-modified electrode => **Signal off** The positively charged L-Cystine assembled on the negatively charged Nf film => ↑ electron transfer	Shi et al., 2014a
CELLS			
Target analyte: RAMOS CELLS			

16 cell*mL^{-1} / 20 to 1000 cells*mL^{-1}	$(Ru(bpy)_2(dcbpy)NHS)$ / DNA toehold-aptamer / DNA primer / Au–Fe_3O_4 TPA (a co-reactant)	***Labeled***. Target induced displacement of the labeled css-DNA => toehold-aptamer / DNA primer / Au–Fe_3O_4 (bio-bar-code) initiate RCA => RCA products hybridized with ECL probe => trapped by magnetic electrode => **Signal on**	Chen et al. (2014b)
50 cells*mL^{-1} / 50 to 1000 cells*mL^{-1}	MBs / aptamers / Au NPs NH_2-linker DNA + reporter DNA / Ru-NHS capture DNA **/ Au electrode**	***Labeled***. Target induced displacement of the labeled css-DNA => **Signal on** Then the solution containing the ECL nanoprobes was separated from the mixture with a magnetic field	Ding et al. 2012
78 cells*mL^{-1} / 100 to 2000 cells*mL^{-1}	Ru-SiNPs / css-DNA / hybridized with SH- aptamer sequence / Au NPs / magnetic beads	***Labeled***. Target induced displacement of the labeled css-DNA => attaching by magnetic beads => re-hybridization of Ru-SiNPs-labeled css-DNA with immobilized onto electrode aptamer => **Signal on**	Yu et al., 2011
Target analyte: K562 LEUKEMIA CELLS			
46 cells mL^{-1} / 1.0×10^2 to 2.0×10^7 cells*mL^{-1}	ZnO@ carbonQDs–concanavalin A / cells / aptamer / nanoporous gold / **SPCE** $K_2S_2O_8$ (a co-reactant)	***Labeled***. Target induced change of interaction between mannose and concanavalin A	Zhang et al., 2013
Target analyte: HL-60 CANCER CELLS			
150 cells mL^{-1} / 200 to 9000 cells*mL^{-1}	DNA functionalized Ag–PAMAM–luminol NCs hybridize with aptamers modified onto magnetic beads / **ITO** H_2O_2 (a co-reactant)	***Labeled css-DNA.*** Target induced displacement of the labeled css-DNA => dual-signaling (**Signal on**. **Signal off**) ECL from g-C_3N_4 nanosheets coated on ITO electrode at 1.25 V (vs SCE) could be quenched by Ag–PAMAM–luminol NCs due to the RET from g-C_3N_4 nanosheets to AgNPs.	Wang et al., 2016
SMALL TARGETS			
Target analyte: ADENOSINE (an endogenous nucleoside)			
1 fM / 1.0 fM to 0.10 μM	Fc-aptamer hybridization with ss-DNA / ITO bipolar electrode Ru / TPA system	***Labeled.*** Target induced displacement of the Fc-aptamer on the cathodic pole that ↓ the oxidation reactions of Ru /TPA system on anode of bipolar electrode => **Signal off** Adenosine was extracted from K562 leukemia cells.	Shi et al., 2014
31 pM /	Ru-SiNPs-SH-ss-DNA1-**A**	***Labeled aptamer and css-DNA.*** Target	Chen

50 nM to 0.1 nM	**u electrode** hybridized with Fc-labeled-ss-DNA2 DBAE (a co-reactant)	induced displacement of the Fc-labeled ss-DNA2=> ↓ of quenching effect **=> Signal on**	et al. 2010
0.5 to 9 ng*mL^{-1} / 0.98 nM to 17.7 nM	GNPs - DNA3 / DNA2 / MCH/ DNA1 / **Au electrode** DBAE (a co-reactant)	***Label-free.*** Target induced structure switching from DNA/DNA duplex to DNA/ target complex => extrication of the intercalated $Ru(phen)_3^{2+}$ => **Signal off.**	Wang et al., 2012
5 nM / 10 nM to 0.1µM	ssc-DNA hybridized with Fc-aptamer-Ru–AuNPs / **Au electrode** TPA (a co-reactant)	***Labeled.*** Target induced dissociation of the ds-DNA => displacement Fc-labeled aptamer => ↑ quenching effect => **Signal off.**	Wang et al., 2010
Target analyte: ADENOSINE TRIPHOSPHATE (a nucleoside triphosphate, used in cells as a coenzyme)			
4.8 pM / 10 pM to 10 nM	GO + MCH $[Ru(bpy)_2(dcbpy)NHS]$ – Apt / AuNPs / **GCE** TPA (a co-reactant)	***Labeled aptamer.*** Target induced extrication of the aptamer from GO modified electrode => ↓ of ECL quenching => ***Signal on*** GO, as a quencher for $[Ru(bpy)_2(dcbpy)NHS]$	Huang et al., 2015
20 pM / 100 pM to1.0 nM	Hybridizing the auxiliary probe with and SH-DNA signaling probe	***Label-free.*** Target induced ATP-ligation => blocking the digestion of ds-DNA by Exonuclease III => intercalation of $Ru(phen)_3^{2+}$ => ***Signal on***	Zhao et al. 2016
0.01 nM / 10.0 to 0.05 nM	tris(bpyRu)-β-CD / NH_2-aptamer / **GCE** DBAE (a co-reactant)	**Label-free.** Target induced restricting of the host–guest interaction between tris(bpyRu)-β-CD and the aptamer => ↓ of tris(bpyRu)-β-CD at the surface of the GCE **=> *Signal off***	Chen et al. 2014a
0.02 nM / 0.05 to 10 nM	$Ru(bpy)_2(cbpy)$ - SH-css-DNA) / **Au electrode** hybridized with the aptamer TPA (a co-reactant)	***Labeled css-DNA.*** Target induced dissociation of ds-DNA => extrication aptamer into the solution => conformation change in a high ionic solution =>↓ of distance of ECL-tag to electrode => ***Signal on***	Yao et al., 2009
0.2 nM / 0.5 nM to 1 µM	Functionalized oligonucleotide / $Ru(phen)_3^{2+}$-ts-DNA composite / **Au electrode** TPA (a co-reactant)	***Label-free***. Target induced dissociation of ts-DNA => partially releasing of intercalated $Ru(phen)_3^{2+}$ => ***Signal off*** Adsorption of the ts-DNA probe to the electrode was stronger than ds-DNA, as a surface-induced perturbation was weaker	Bu et al., 2013
1.0 nM / 5 nM to 0.5 mM	Ru / Aptamer / SWCNH / **GCE** TPA (a co-reactant)	***Label-free.*** Target induced desorption $Ru(bpy)_3^{2+}$ from SWCNH => ↓ of ECL quenching => **Signal on**. Ru-complex may be adsorbed onto the electrode surface via the electrostatic	Liu et al., 2015

		attraction. SWCNH were employed both as a quencher and scaffold.	
6 nM / 0.018 to 90.72 mM	Avidin-QDs - biotin-css-DNA hybridized with MCH / SH-aptamer / **Au electrode** $K_2S_2O_8$ (a co-reactant)	***Labeled css-DNA.*** Target induced dissociation of ds-DNA => extrication of QDs–labeled-css-DNA => **Signal off**	Huang et al., 2010
Target analyte: 17β-ESTRADIOL (an estrogen)			
1.1 pM / 0.01 to 10 nM	Ru (adsorbed onto the aptamer) + cDNA / SH-aptamer / **Au electrode** TPA (a co-reactant)	***Label-free***. Target induced dissociation of aptamer and complementary strand hybrid => extrication of adsorbed Ru into solution => **Signal off**	Zhang et al., 2014
Target analyte: 2,4,6-TRINITROTOLUENE (an organic explosive)			
0.0036 $ng*mL^{-1}$ / 0.01 to 100 $ng*mL^{-1}$	cis-$RuCl_2(bpy)_2$–GO / aptamer–AuNPs / **ITO electrode** TPA (a co-reactant)	***Label-free.*** Aptamer–target induced aggregation of mono-dispersed AuNPs => neutralization of negative charge of AuNPs => AuNPs extrication from Ru–GO => ↓ quenching effect => **Signal on**. AuNP, as a quencher.	Yu et al., 2013
6.3×10^{-13} g/mL 1.0×10^{-12} – 1.0×10^{-9} g*mL	Biotin-aptamer-SA-luminol-AgNPs-GO / CS-A-H-GNs/ **ITO electrode** H_2O_2 (a co-reactant)	***Label-free.*** Aptamer–target interaction ↓ adsorption of luminol onto the modified electrode => **Signal off.** A-H-GNs and luminol-AgNPs-GO exhibited excellent ECL activity. *Positively* charged CS-A-H-GNs (+55.3 mV zeta potential) were modified on the surface of ITO electrode. *Negatively* charged apta-biotin-SA-luminol-AgNPs-GO (-22.7 mV zeta potential)	Li et al., 2015
Target analyte: BISPHENOL A (an organic synthetic compound)			
0.037 $ng*mL^{-1}$ /	Aptamer / AuNPs Hybridized with css-DNA-NaYF4:Yb,	***Labeled css-DNA.*** Target induced dissociation of ds-DNA =>	Guo et al.,

0.05 to 100 ng*mL^{-1}	Er/Mn upconversion nanoparticles	extrication of upconversion nanoparticles– labeled-css-DNA into the solution => **Signal off**	2016
0.05 ng*mL^{-1} / 0.05 to 200 ng*mL^{-1}	[(PEI/PSS)$_4$(PEI/aptamer)$_6$] / Au–g-C_3N_4 film / **GCE** $S_2O_8^{2-}$ (a co-reactant)	***Label-free.*** Target induced ↑ of the permeability of polyelectrolyte film => **Signal-on** Au–g-C_3N_4 was employed as an ECL-emitter	Chen, 2015b
Target analyte: CHLORAMPHENICOL (antibiotic) **and MALACHITE GREEN** (organic dye)			
0.03 nM / 0.1 to 120 nM	L-Au NPs / css-DNA / SH-aptamer / **SPCE1** CA + CdS QDs / DNA2 / **SPCE2** H_2O_2 (a co-reactant)	***Label-free.*** Target induced reducing of the quenching effect => **Signal on.** Chlorogenic acid (CA), as a quencher. Ratiometric array consisting of two spatial resolved working electrodes. ΔECL signals between ECL at **SPCE1** and ECL at **SPCE2** => reduce the matrix environmental interference	Feng et al., 2016
CAP: 0.07 nM / 0.2 to 150 nM MG: 0.03 nM / 0.1 to 100 nM	**CAP**: css-DNA / Luminol-gold nanoparticles / hybridized with CA / PEI/ Aptamer / **SPCE2** (anode) H_2O_2 (a co-reactant) **MG**: css-DNA / CdS QDs hybridized with Cy5-PEI-aptamer **SPCE** 1 / (cathode); H_2O_2 (a co-reactant)	***Labeled***. Aptamer–target interaction reduces quenching effect => **Signal on** ECL aptasensor array. Simultaneous detection of MG and CAP in one single assay. Cy5, as a quencher of CdS QDs ECL. CA – as a quenchers of L-Au NPs. PEI, as a bridging agent.	Feng et al., 2015
Target analyte: KANAMYCIN (aminoglycoside antibiotics)			
45 pM / 0.15 nM to 170 mM	Au@nano-C_{60} / Hemin / G-quadruplex DNAzymes. poly-L-histidine (a co-reactant)	***Label-free.*** "on-off-on" switch system ❶ poly-L-histidine, as a coreactant of $S_2O_8^{2-}O_2$ system => ***Signal on*** ❷ Quenching effect of hemin / G-quadruplex DNAzymes towards $S_2O_8^{2-}O_2$ => ***Signal off*** ❸ Aptamer–target interaction => ↓ quenching effect => ***Signal on***	Zhao et al., 2015
Target analyte: COCAINE (stimulant)			
0.2 pM / (3-fold)	$Ru(phen)_3^{2+}$ / Apt / **Au electrode** TPA (a co-reactant)	***Label-free.*** Target induced formation of a duplex in the aptamer => $Ru(phen)_3^{2+}$ intercalation => **Signal on**	Zhao et al., 2011
Target analyte: Ochratoxin A (mycotoxin)			

10 fM / 0.00005 – 100 nM	HT / css-DNA hybridized with aptamer / AuNP / **GCE**	***Label-free.*** Target induced dissociation of the ds-DNA => displacement of the aptamer into the solution => producing of LAMP amplicon => ↓ $Ru(phen)_3^{2+}$ interlation into amplicons within a fixed $Ru(phen)_3^{2+}$ amount => ***ECL Signal on***. The ECL indictor $Ru(phen)_3^{2+}$ binding to amplicons caused the reduction of the ECL intensity due to the slow diffusion of $Ru(phen)_3^{2+}$ –amplicons complex to the electrode surface.	Yuan et al., 2014b
1.24 pM / 2.47 pM to 24.7 nM	SH-Aptamer / core-shell Fe_3O_4@Au MBs hybridized with css-DNA-NGQDs @SiO_2 NPs $K_2S_2O_8$ (a co-reactant)	***Labeled css-DNA.*** Target induced dissociation of ds-DNA => extrication of the NGQDs@SiO_2 NPs - labeled-css-DNA into the solution **=> Signal off** Solid-state ECL platform. NGQDs@SiO_2 NPs have been prepared through a typical Stöber method. Dual channel OTA detection: solid-state ECL and homogeneous FL. The FL assay exhibits a widerdynamic range due to the homogeneous detection	Wang et al., 2015
1.58 pM / 4-fold	Aptamer-ReCJf exonuclease / ethanolamine / ds-DNA/CdTe–MWCNT–CS / **GCE** Triethylamine (a co-reactant)	***Label-free.*** Target induced removal of the biotin–aptamers from the electrode surface via ***exonuclease-catalyzed recycling*** and reuse of OTA, which prevents the attachment of SA–ALP through biotin–SA interaction. The ET from the excited state CdTe QD ([CdTe]n) to the electro-oxidized species of the enzymatic product of –alkaline is thus inhibited and the QD ECL emission is restored. The restoration of the ECL emission is dramatically amplified due to the	Yang et al., 2014

		exonuclease-catalyzed recycling and reuse of OTA => **Signal on**
Target analyte: Pb^{2+}		
0.35 pM / 1 pM to 0.1 µM	Aptamer hybridized with PTC-NH_2 AuNPs@nano-C_{60} / **GCE**	***Label-free.*** Target induced generation of the G-quadruplex structure => PTC-NH_2 release from the electrode surface => **Signal off.** RET ECL system from $O_2/S_2O_8^{2-}$ (air-saturated solution) to PTC-NH_2. (ECL acceptor).
37.4 pM / 0.2 nM – 50 nM	CdS QDs / hairpin structures-aptamer / **Au electrode** $K_2S_2O_8$ (a co-reactant)	***Labeled.*** Target induced generation of the G-quadruplex structure => more 3'-NH_2 would exposed because of the transformation of the DNA sequence, which could bind too more CdS QDs => **Signal on.**
10.8pM / 0.2 nM to 10 nM	CdTe QDs + Fe_3O_4–Au-hairpin structures-aptamer / **MCGE** $K_2S_2O_8$ (a co-reactant)	***Label-free. A*** Target induced generation of the G-quadruplex structure => the ''stem-loop'' structure of the hairpin DNA2 exposed more basic groups which could bind too more CdS QDs => **Signal on.**

Highlights

► Electrochemiluminescent aptasensors have been comprehensively reviewed.
► Main strategies of ECL aptamer-based assay are summarized.
► Signal amplification strategies are presented.
► The challenges and opportunities are discussed

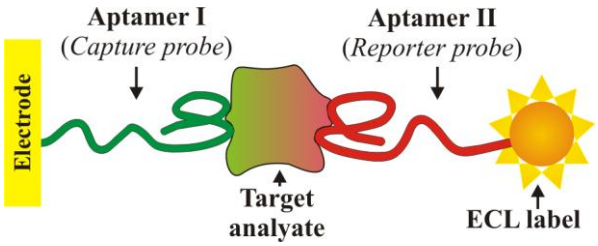

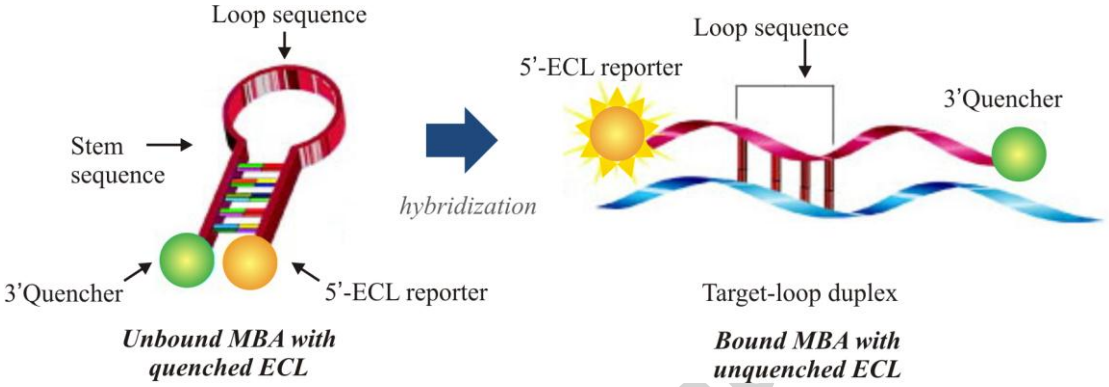

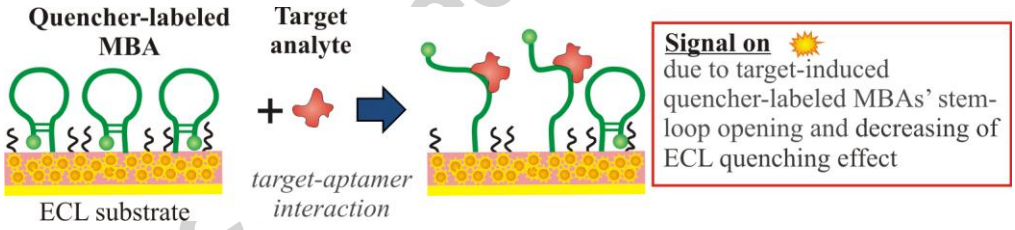

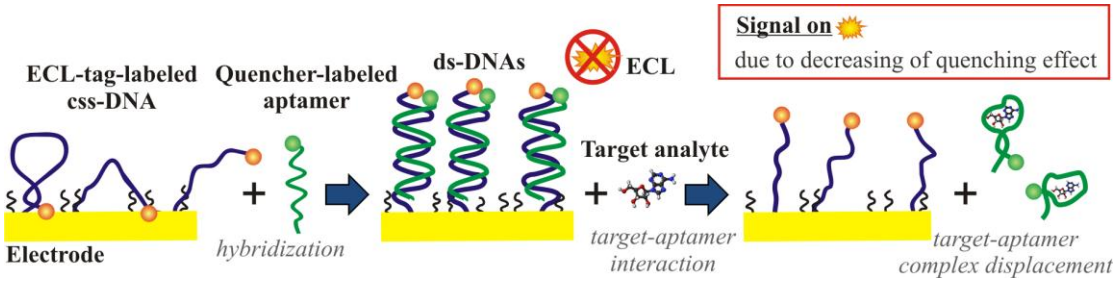

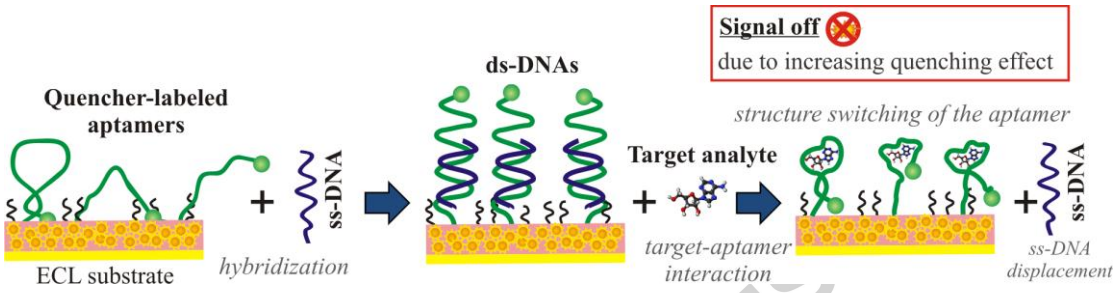

Before target-aptamer interaction

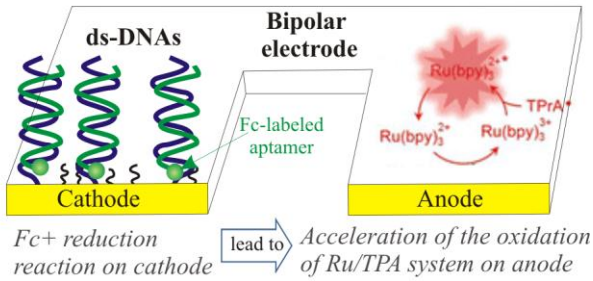

After target-aptamer interaction